Production of pions, kaons, and protons as a function of the relative transverse activity classifier in pp collisions at $$ \sqrt{s} $$ = 13 TeV

(ALICE Collaboration) Acharya, Sheryasi; ...; Erhardt, Filip; ...; Gotovac, Sven; ...; Jerčić, Marko; ...; Karatović, David; ...; ...

Journal article, Published version
Rad u časopisu, Objavljena verzija rada (izdavačev PDF)

Permanent link / Trajna poveznica: https://urn.nsk.hr/urn:nbn:hr:217:877226

Download date / Datum preuzimanja: **2025-01-28**

Production of pions, kaons, and protons as a function of the relative transverse activity classifier in pp collisions at $\sqrt{s} = 13$ TeV

The ALICE collaboration

E-mail: alice-publications@cern.ch

ABSTRACT: The production of $\pi^{\pm}$, $K^{\pm}$, and $(\overline{p})p$ is measured in pp collisions at $\sqrt{s} = 13$ TeV in different topological regions of the events. Particle transverse momentum (p_{T}) spectra are measured in the "toward", "transverse", and "away" angular regions defined with respect to the direction of the leading particle in the event. While the toward and away regions contain the fragmentation products of the near-side and away-side jets, respectively, the transverse region is dominated by particles from the Underlying Event (UE). The relative transverse activity classifier, $R_{T} = N_{T}/\langle N_{T} \rangle$, is used to group events according to their UE activity, where N_{T} is the measured charged-particle multiplicity per event in the transverse region and $\langle N_{T} \rangle$ is the mean value over all the analysed events. The first measurements of identified particle p_{T} spectra as a function of R_{T} in the three topological regions are reported. It is found that the yield of high transverse momentum particles relative to the R_{T}-integrated measurement decreases with increasing R_{T} in both the toward and the away regions, indicating that the softer UE dominates particle production as R_{T} increases and validating that R_{T} can be used to control the magnitude of the UE. Conversely, the spectral shapes in the transverse region harden significantly with increasing R_{T}. This hardening follows a mass ordering, being more significant for heavier particles. Finally, it is observed that the p_{T}-differential particle ratios $(p + \overline{p})/(\pi^{+} + \pi^{-})$ and $(K^{+} + K^{-})/(\pi^{+} + \pi^{-})$ in the low UE limit ($R_{T} \to 0$) approach expectations from Monte Carlo generators such as PYTHIA 8 with Monash 2013 tune and EPOS LHC, where the jet-fragmentation models have been tuned to reproduce $e^{+}e^{-}$ results.

Contents

1 Introduction

In recent years, proton-proton (pp) and proton-lead (p-Pb) collisions, commonly denoted as small collision systems, have attracted the heavy-ion community's attention due to several measurements in high-multiplicity pp and p-Pb collisions, which show similar features as those observed in heavy-ion collisions. Observations of radial [1–4] and anisotropic [5, 6] flows (collective phenomena), as well as strangeness enhancement [1, 7, 8] in heavy-ion collisions, are associated with the formation of the strongly interacting quark-gluon plasma (QGP). However, these signatures have also been observed in pp and p-Pb collisions [2, 4, 8, 9]. In particular, the p_{T}-differential baryon-to-meson ratios in small collision systems showcase radial-flow like effects when studied as a function of the charged particle multiplicity of the event [2, 3]. In order to pin down the origins of the effects observed in small collision systems, it has been proposed to study particle production as a function of the Underlying Event (UE) activity [10]. The UE is defined as the particles that do not originate from the fragmentation products of the partons produced in the hardest scattering. It consists of the set of particles arising from initial- and final-state radiation, beam remnants and multiple parton interactions (MPIs) [11]. In the context of MPI models, the measurement of identified particle yields and ratios as a function of the UE activity allows one to measure event properties in an MPI-suppressed (-enhanced) environment. Moreover, as shown in [12], these measurements can also provide insights into possible effects that give similar signatures as radial flow but are produced by jet hardening with increasing multiplicity.

At the LHC energies, particles and anti-particles are produced in equal amounts [13]. In the remaining of this paper and unless stated otherwise, the notation π, K and p is adopted to refer to $(\pi^+ + \pi^-)$, $(K^+ + K^-)$, and $(p + \bar{p})$, respectively. In this study, the production of π, K, and p is studied as a function of the UE activity in pp collisions at centre-of-mass energy, $\sqrt{s} = 13\,\text{TeV}$. The UE is examined using the event topology defined by the leading charged particle in the event, which is defined as the charged particle with the highest transverse momentum in the range $5 \leq p_\text{T}^\text{leading} < 40\,\text{GeV}/c$, and reconstructed in the pseudorapidity interval $|\eta| < 0.8$. The lower $p_\text{T}^\text{leading}$ threshold corresponds to the onset of the UE plateau in the transverse region (transverse to the direction of the leading particle) [14–17]. In the plateau region, quantities such as the average charged-particle density, $\langle N_\text{ch} \rangle$, and the average transverse momentum sum, $\langle \sum p_\text{T} \rangle$, have little dependence on the p_T of the leading particle or jet. This study uses a lower threshold on the $p_\text{T}^\text{leading}$ of $5\,\text{GeV}/c$ to guarantee that the multiple soft scatterings that contribute to the UE are largely independent of the $p_\text{T}^\text{leading}$. In [18] a slow rise of the UE plateau is reported. This can be explained by additional contributions from wide-angle radiation associated with the hard scattering. Since wide-angle contamination becomes significant for jet $p_\text{T} > 50\,\text{GeV}/c$ [18], an upper limit on $p_\text{T}^\text{leading}$ of $40\,\text{GeV}/c$ is used to reduce its effects.

To study the particle production associated with different underlying physics mechanisms, the conventional division of the azimuthal (φ) plane into regions relative to the direction of the leading particle [19] is used (see figure 1). The observables reported in this paper are measured in three different topological regions, the toward, transverse, and away regions. These are defined based on the absolute difference in azimuthal angle between the leading and associated particles, $|\Delta\varphi| = |\varphi^\text{leading} - \varphi|$. The associated particles are measured in the kinematic range $0.15 \leq p_\text{T} < 5\,\text{GeV}/c$ and $|\eta| < 0.8$. The toward, transverse, and away regions are defined by $|\Delta\varphi| < 60°$, $60° \leq |\Delta\varphi| < 120°$, and $|\Delta\varphi| \geq 120°$, respectively. The particle production in the toward and away regions contains the constituents of the leading and away-side jets, respectively, the transverse region is mainly sensitive to multiple parton interactions and initial- and final-state radiations.

The UE activity is quantified using the relative transverse activity classifier R_T [10], which is defined as $N_\text{T}/\langle N_\text{T} \rangle$, where N_T is the measured charged-particle multiplicity per event in the transverse region and $\langle N_\text{T} \rangle$ is the mean value over all the analysed events. By construction, R_T cleanly separates events with "higher-than-average" UE from "lower-than-average" ones irrespective of the centre-of-mass energy. Of particular interest is whether events with very low UE activity, which are dominated by the jet activity, exhibit particle ratios and spectra consistent with fragmentation models tuned to e^+e^- data and whether events with high UE activity exhibit any clear signs of flow or other collective effects [10]. Finally, it is worth mentioning that this study is complementary to the measurements made using transverse spherocity, in which global event properties are studied for jet-like and isotropic topologies [20, 21].

The structure of the paper is as follows: in section 2, the data analysis is described, section 3 discusses the systematic uncertainties, and in section 4, the results are presented. Finally, in section 5, the conclusions are given.
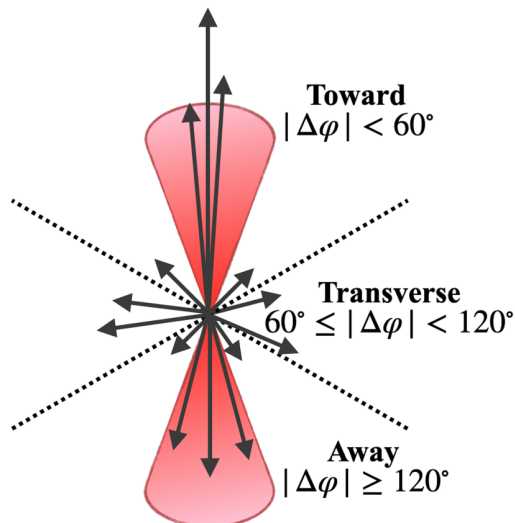
Figure 1. Illustration of the toward, transverse, and away regions in the azimuthal angle plane with respect to the direction of the leading particle. The leading particle is represented with the longest upright arrow. The UE is represented with the small arrows transverse to the leading particle. The red cones represent the jet and away-side jet.

2 Analysis procedure

2.1 Event and track selection

This study was carried out with the data collected in pp collisions at $\sqrt{s} = 13$ TeV by the ALICE Collaboration during the LHC runs from 2016 and 2018. A detailed description of the ALICE apparatus and its performance can be found in [22, 23]. The subdetectors used in this analysis are the V0 [24], the Inner Tracking System (ITS) [25], the Time Projection Chamber (TPC) [26], and the Time-Of-Flight (TOF) [27]. These subdetectors are located inside a $B = 0.5$ T solenoidal magnetic field. The V0 detector consists of two arrays of 32 scintillators each, covering the forward (V0A, $2.8 < \eta < 5.1$) and backward (V0C, $-3.7 < \eta < -1.7$) pseudorapidity regions. The ITS is the innermost barrel detector. It consists of six cylindrical layers of high-resolution silicon tracking detectors: the two innermost layers of the Silicon Pixel Detector (SPD) provide a digital readout and are also used as a trigger detector. The Silicon Drift Detector (SDD) and the Silicon Strip Detector (SSD) compose the four outer layers of the ITS. Together, they provide the amplitude of the charge signal, which is used for particle identification through the measurement of the specific energy loss $(\mathrm{d}E/\mathrm{d}x)$. The TPC is the primary detector for tracking and particle identification. It is a large cylindrical drift detector with a diameter and length of about 5 m, which covers the pseudorapidity range $|\eta| < 0.8$ with full-azimuth coverage. Particle identification is accomplished via the measurement of the $\mathrm{d}E/\mathrm{d}x$. In pp collisions the resolution of the $\mathrm{d}E/\mathrm{d}x$ is about 5 %. The TOF is a large-area array of multigap resistive plate chambers (MRPC), which surrounds the interaction point and covers the pseudorapidity region $|\eta| < 0.9$ with full-azimuth coverage. The time-of-flight is measured as the difference between the particle arrival time and the event collision time.

The event selection in this study follows those of the previous studies to measure the production of π, K, and p as a function of the charged-particle multiplicity in [3, 28]. The minimum-bias trigger requires signals in both V0A and V0C scintillators in coincidence with the arrival of the proton bunches from both directions. The primary vertex position is reconstructed using global tracks (reconstructed using ITS and TPC information). For events with too few tracks to compute the vertex position, the primary vertex from SPD tracklets (reconstructed using only SPD information) is used instead. Events are required to have a vertex position along the z-axis (parallel to the beam axis) in $|z| < 10$ cm, where $z = 0$ corresponds to the centre of the detector. The out-of-bunch pileup is rejected offline using the timing information from the two V0 subdetectors. Furthermore, events with multiple interaction vertices reconstructed are rejected. Finally, events are required to have a leading particle with $5 \leq p_{\mathrm{T}}^{\mathrm{leading}} < 40 \,\mathrm{GeV}/c$. The total number of events after event and vertex selections amounts to about 827 million, while the number of analysed events with a leading particle is about 8.1 million.

The distributions presented in this study correspond to primary charged particles, which are defined as particles with a mean proper lifetime τ larger than $1\,\mathrm{cm}/c$, which are either produced directly in the interaction or from decays of particles with τ smaller than $1\,\mathrm{cm}/c$, excluding particles produced in interactions with material [29]. Primary charged particles are reconstructed using the ITS and TPC detectors, which provide measurements of the track transverse momentum and azimuthal angle. In particular, tracks are required to cross at least 70 TPC pad rows. They are also required to have at least two hits in the ITS, out of which at least one is in the SPD layers. The fit quality for the ITS and TPC track points must satisfy $\chi^2_{\mathrm{ITS}}/N_{\mathrm{hits}} < 36$ and $\chi^2_{\mathrm{TPC}}/N_{\mathrm{clusters}} < 4$, respectively, where N_{hits} and N_{clusters} are the number of hits in the ITS and the number of clusters in the TPC associated to the track, respectively. Finally, tracks are also required to have a transverse momentum larger than $0.15\,\mathrm{GeV}/c$ and to be reconstructed in $|\eta| < 0.8$. To limit the contamination from secondary particles, a selection on the distance of closest approach (DCA) to the reconstructed vertex in the direction parallel to the beam axis (z) of $|\mathrm{DCA}_z| < 2\,\mathrm{cm}$ is applied. Also, a p_{T}-dependent selection on the DCA in the transverse plane (DCA_{xy}) of the selected tracks to the primary vertex is applied. Moreover, tracks associated with the decay products of weakly decaying kaons ("kinks") are rejected. In ALICE, the set of tracks reconstructed with the above-mentioned selection criteria is commonly referred to as "global tracks".

The use of global tracks yields a significantly non-uniform efficiency as a function of the azimuthal angle and pseudorapidity. In order to obtain a high and uniform tracking efficiency together with good momentum resolution, "hybrid tracks" are used [30, 31]. Hybrid tracks correspond to the union of two different sets of tracks selected with complementary criteria: (i) tracks containing at least one space-point reconstructed in one of the two innermost layers of the ITS (global tracks) and (ii) tracks without an associated hit in the SPD for which the position of the reconstructed primary vertex is used in the fit of the tracks. Hybrid tracks are used to select the leading particle, as well as to measure N_{T} and the p_{T} spectra. Furthermore, in order to select high-quality high-p_{T} tracks, a selection based on the geometrical track length (L) is applied [32]. This selection criterion excludes the information from the readout pads at the TPC sector boundaries ($\approx 3\,\mathrm{cm}$ from the sector edges).

Analysis	p_T ranges (GeV/c)		
	π	K	p
TPC	0.25–0.7	0.3–0.6	0.45–1.0
TOF	0.7–3.0	0.6–3.0	1.0–3.0
rTPC	2.0–5.0	3.0–5.0	3.0–5.0

Table 1. The name of the analysis technique and the transverse momentum ranges in which π, K and p are identified.

2.2 Particle identification

ALICE's tracking and particle identification (PID) capabilities allow measuring the transverse momentum spectra of π, K, and p over a wide range of transverse momentum. In this study the p_T spectra are measured in the $p_T < p_T^{\text{leading}}$ interval, using the standard particle identification techniques which have been reported in previous ALICE publications [3, 28, 33–35]. Table 1 shows the three techniques used for the PID and the p_T intervals each method covers.

At low p_T, the average energy loss, $\langle dE/dx \rangle$, is proportional to $1/(\beta\gamma)^2$ and the relatively large $\pi - $ K and p $-$ K separation power makes it possible to perform particle identification in this region on a track-by-track basis [28]. Thus in the TPC analysis, the relative particle abundances, which are defined as the measured fractions of π, K, and p with respect to all the measured primary charged particles are obtained from fitting n_σ distributions in narrow intervals of transverse momentum. For each track, the n_σ is defined as the difference between the measured and expected dE/dx values normalised to the resolution, $n_\sigma = (dE/dx_{\text{measured}} - \langle dE/dx_{\text{expected}} \rangle)/\sigma$. While the signal of π and p can be fitted with a Gaussian parameterisation, the one for K uses the sum of two Gaussians as parameterisation to take into account the contamination by electrons.

In the TOF analysis, the particle abundances are also measured on a track-by-track basis by fitting the measured β,[1] distributions in momentum intervals. In the interval $1 < p < 2\,\text{GeV}/c$, the $\pi - $ K and p $-$ K separation power of hadron identification is large enough [28] such that one can perform single fits to the signal of π, K, and p using a Gaussian parameterisation convoluted with an exponential tail. The parameters (μ, σ and ξ, where μ and σ represent the mean and standard deviation of the Gaussian parameterisation, and ξ represents the β value at which the exponential tail begins) of the single fits are extracted from data in $1 < p < 2\,\text{GeV}/c$ and are used to extrapolate to higher momentum values. Finally, the extrapolated functional forms are used to fit the β distributions with the sum of three contributions to describe the signals of the three species simultaneously.

In the rTPC analysis, the method described in [33–35] is used. In the relativistic rise region of the TPC ($3 \lesssim \beta\gamma \lesssim 1000$), the $\langle dE/dx \rangle$ increases as $\log(\beta\gamma)$ and the $\pi - $ K and p $-$ K separation power for hadron identification is almost constant [28]. The knowledge of these two features makes it possible to perform a two-dimensional fit of the correlation between dE/dx and momentum. In order to accomplish this, the first step

---

[1]$\beta = L/c\Delta t$, where L is the track length and Δt is the measured time-of-flight.

is to parameterise the Bethe-Bloch and resolution curves in the relativistic rise region. The Bethe-Bloch parameterisation provides the relation between the $\langle dE/dx \rangle$ and $\beta\gamma$, and the parameterised resolution gives the relation between $\sigma_{dE/dx}$ and $\langle dE/dx \rangle$. For the parameterisation, high-purity samples of identified hadrons are used, namely $p(\bar{p})$ and $\pi^{\pm}$ from $\Lambda(\bar{\Lambda})$ and K_S^0 decays, respectively, and $e^{\pm}$ from γ-conversions [33–35]. Once the Bethe-Bloch and resolution curves are parameterised, they are used to perform the two-dimensional fit. The two-dimensional fit is only used to improve the Bethe-Bloch parameterisation in the transition to the plateau region. Then, the particle ratios are obtained from one-dimensional fits to the dE/dx distributions in momentum intervals using the sum of four Gaussians as a fit function to describe simultaneously the signal of π, K, p, and e, where the μ and σ of each of the Gaussian distributions are fixed based on the $\langle dE/dx \rangle(\beta\gamma)$ and $\sigma_{dE/dx}(\langle dE/dx \rangle)$ obtained with the above procedure.

2.3 Corrections

The p_T spectra of π, K, and p are corrected for acceptance and reconstruction inefficiency. The spectra measured with the TOF detector are also corrected for TPC–TOF matching inefficiency. The acceptance and efficiencies are obtained from simulations using the PYTHIA8 Monte Carlo event generator with the Monash 2013 tune (indicated as PYTHIA8 Monash in the following) [36]. Subsequently, the propagation of simulated particles through the ALICE apparatus is carried out using GEANT3 [37]. The simulated events are reconstructed using the same algorithms as for the data. The obtained acceptance and reconstruction efficiencies are independent of the charged-particle multiplicity. Hence, the R_T-integrated values are applied for all the R_T classes. As GEANT3 does not fully describe the interaction of low-momentum $\bar{p}$ and K^- with the detector material, an additional correction factor to the efficiency for these two particles is estimated with GEANT4 [38] and FLUKA [39], respectively. These corrections are the same as the ones applied in [3].

The p_T spectra of π and p contain a large contribution from secondary particles from interactions in the material and particle decays ($\pi^{\pm}$ from K_S^0 and $p(\bar{p})$ from Λ and Σ^+). Since the strangeness production is underestimated in the Monte Carlo event generators, a data-driven approach is used to estimate the fraction of non-primary particles as a function of p_T so that it can be subtracted from the measured spectra. The estimation of this correction is based on a multi-template fit method to describe the measured DCA_{xy} distributions [40]. In practice, three Monte Carlo templates representing the expected shapes of DCA_{xy} distributions of primary particles, secondaries from weak decays, and secondaries from interactions in the material are used to fit the data DCA_{xy} distributions. The fits are performed in $|DCA_{xy}| \leq 3$ cm and in p_T bins. Since the TOF analysis only uses tracks matched with the TOF detector, these corrections are estimated separately for the low- and intermediate-p_T regions. At $p_T = 0.45$ GeV/c the contribution from non-primary $\pi^+(p)$ was found to be about 4%(20%) while at $p_T = 2.0$ GeV/c it decreases to about 1%(4%). Furthermore the correction decreases asymptotically at higher p_T. Therefore, the correction for the TOF is extrapolated to higher p_T and then applied.
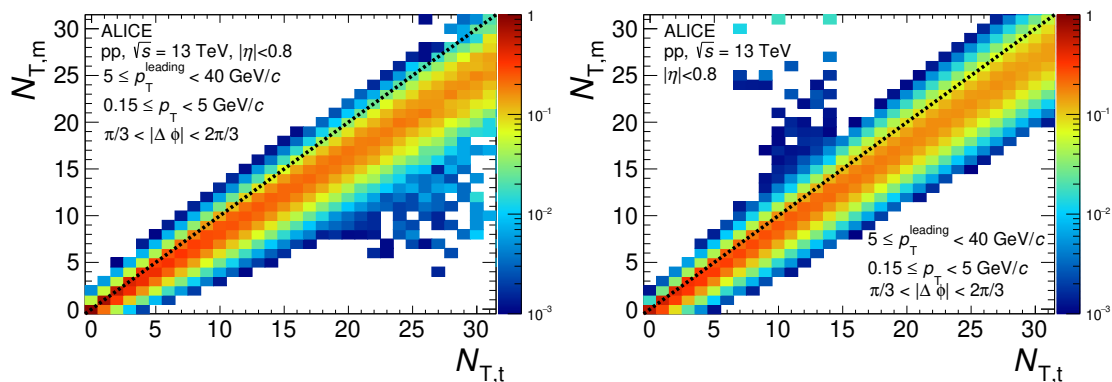
Figure 2. (Left) Correlation between the true $N_{\text{T,t}}$ and the measured $N_{\text{T,m}}$ multiplicity in the transverse region. (Right) Unfolding matrix M1_{tm}. The iteration step of the unfolding matrix corresponds to the third.

2.4 Unfolding the charged-particle multiplicity distributions

The charged-particle multiplicity in the transverse region, N_{T}, is used to characterise the event activity. However, the limited acceptance and finite resolution of the detector cause a smearing of the measured charged-particle multiplicity distribution $Y(N_{\text{T,m}})$. This section introduces the one-dimensional unfolding method to correct for these detector effects and efficiency losses. The adopted approach is based on the iterative Bayesian unfolding method by G. D'Agostini [41]. Bayesian unfolding requires the knowledge of the smearing matrix S_{mt}, which comprises information about the limited acceptance and finite resolution. It represents the conditional probability $P(N_{\text{T,m}}|N_{\text{T,t}})$ of an event with the true multiplicity $N_{\text{T,t}}$ to be measured as one with multiplicity $N_{\text{T,m}}$. Figure 2 (left) shows the smearing matrix obtained with simulated events using PYTHIA8 Monash. The values along the diagonal of the smearing matrix represent the probability that a measured event is reconstructed with the true number of particles. At the same time, the off-diagonal elements give the probability that fewer or more particles are reconstructed due to detector inefficiencies and background, e.g., secondary particles misidentified as primary particles.

The one-dimensional unfolded distribution $Y(N_{\text{T,t}})$ is given as the linear combination between the elements of the unfolding matrix M1_{tm} (see the right panel of figure 2) and the measured distribution,

$$Y(N_{\text{T,t}}) = \sum_{\text{m}} \text{M1}_{\text{tm}} Y(N_{\text{T,m}}), \quad \text{where} \quad \text{M1}_{\text{tm}} = \frac{P(N_{\text{T,m}}|N_{\text{T,t}})\, P_0(N_{\text{T,m}})}{\sum_t P(N_{\text{T,m}}|N_{\text{T,t}})\, P_0(N_{\text{T,m}})}. \quad (2.1)$$

$P_0(N_{\text{T,m}})$ represents a prior probability distribution. It can be any arbitrary distribution at the start of the unfolding process. Here, the measured multiplicity distribution is used as the prior distribution. An updated prior distribution,

$$\widehat{P}(N_{\text{T,t}}) = \frac{Y(N_{\text{T,t}})}{\sum_{N_{\text{T,t}}} Y(N_{\text{T,t}})}, \quad (2.2)$$

is obtained from the second iteration and onwards. Thus, the unfolding matrix is improved as the prior distribution is updated. Finally, a new unfolded distribution closer to the

true one can be obtained using eq. (2.1) with the updated $M1_{tm}$. The smearing in figure 2 left shows very few events below the main correlation band between $7 < N_{T,t} < 15$ and $15 < N_{T,m} < 30$. This small population comes from statistical fluctuations of the response matrix. Since the unfolding matrix $M1_{tm}$ is proportional to $P(N_{T,m}|N_{T,t})$, these events show up in $M1_{tm}$ in the intervals $22 < N_{T,t} < 30$ and $7 < N_{T,m} < 17$, as can be seen in figure 2 right. However, given their very small contribution, they are not affecting the unfolding process.

This iterative process makes the unfolded distribution to converge to the true one eventually. However, it also compounds the effects of statistical uncertainties in the smearing matrix. Therefore, a larger number of iterations does not guarantee a better result: eventually, the true distribution might be contaminated by statistical fluctuations [42]. In order to decide when to stop the iterations, the χ^2/N_{df} between the unfolded and the true distribution as a function of the number of iterations is computed for a Monte Carlo generated sample. The minimum value of the ratio χ^2/N_{df} indicates when to stop the iterative process. This study found that the optimal number of iterations is three.

2.5 Unfolding the p_T spectra

Unfolding the transverse momentum spectra as a function of the multiplicity is treated differently depending on the topological region. The toward and away regions are straightforward cases as there is no overlap between the tracks used for the spectra and the tracks used for the multiplicity calculation as the latter is measured in the transverse region. Therefore, the one-dimensional unfolding matrix $M1_{tm}$ is directly applied in these two regions. This also makes it trivial to see that the same unfolding matrix can be used for all identified particle spectra. Hence, the fully corrected p_T spectra as a function of $N_{T,t}$ are obtained in a two-step procedure:

1. Correct the raw p_T spectra at particle level for tracking inefficiency and secondary particle contamination. The efficiency correction is applied here as the one-dimensional unfolding only affects the classification of the events.

2. Apply the one-dimensional unfolding matrix. The spectra as a function of $N_{T,t}$ are given by: $\frac{dY(N_{T,t})}{dp_T} = \sum_m M1_{tm} \frac{dY(N_{T,m})}{dp_T}$

The transverse region requires a more elaborate method since both p_T spectra and multiplicity are measured using the same tracks. In other words, one is no longer dealing with the problem of rearranging events but rather how tracks should be unshuffled to match the true transverse momentum distributions. This poses a multi-dimensional problem with two dimensions associated to the true and measured multiplicities and two additional dimensions (true and measured yields) for each p_T bin. Instead of performing the full multi-dimensional unfolding, an approximate method is employed in which the multiplicity smearing matrix is assumed to be independent of the transverse momentum. This is a very good approximation as the efficiency is essentially flat in p_T for the track selection and p_T ranges used here. In this approach, a new response matrix is obtained by multiplying every column of the

original multiplicity response matrix with the respective number of measured particles as weights. After row-wise normalisation, the desired track smearing matrix is obtained.

The unfolding is done bin-by-bin in p_T with this modified response matrix. For a particular transverse momentum bin, the measured multiplicity distribution is unfolded using the iterative unfolding procedure described in section 2.4. This approach yields unfolding matrices that depend on the transverse momentum. Henceforth, these matrices will be called $M2_{tm}(p_T)$. It should be stressed that this method works here because the tracking efficiency does not depend strongly on the transverse momentum for hybrid tracks and because the same tracks to measure N_T are used to obtain the spectra.

Similar to the toward and away regions, the two-step procedure is followed to obtain the fully corrected transverse momentum spectra. The only difference is that in the transverse region the p_T-dependent $M2_{tm}(p_T)$ matrices are used

$$\frac{dY(N_{T,t}, p_T)}{dp_T} = \sum_m M2_{tm}(p_T) \frac{dY(N_{T,m}, p_T)}{dp_T}.$$ (2.3)

The method described above unfolds the spectra of all charged particles and yields the unfolding matrices $M1_{tm}$ and $M2_{tm}(p_T)$. When unfolding the spectra of identified particles (for example, π in the transverse region), eq. (2.3) is applied using the $M2_{tm}(p_T)$ matrices from charged particles and then exchanging $dY(N_{T,m}, p_T)/dp_T$ for $dY^\pi(N_{T,m}, p_T)/dp_T$. The unfolding of π spectra in the toward and away regions is done with the same strategy but using $M1_{tm}$ instead.

3 Systematic uncertainties

In this section, the estimation of the systematic uncertainties is described. The systematic uncertainties on the p_T spectra are divided into two categories, R_T-dependent and R_T-independent uncertainties. The total systematic uncertainty on the p_T spectra is given as the sum in quadrature of all the individual sources of uncertainty.

R_T-dependent systematic uncertainties. The unfolding method described in section 2.4 shows deficiencies, mainly when unfolding the p_T spectra for low multiplicities in the transverse region. To account for these deficiencies, the following contributions to the systematic uncertainty on the N_T distribution are considered:

- Monte Carlo (MC) non-closure: PYTHIA8 Monash is the default tune for the generation of the multiplicity response matrix and N_T distributions with and without the detector's efficiency losses. The unfolded N_T spectrum from the simulation is compared to the generated one. Thus, any statistically significant difference between the generated and unfolded distributions is referred to as MC non-closure and is added in quadrature to the total systematic uncertainty. During the unfolding procedure, the MC closure improves with the number of iterations, with an optimal number of three, which leads to a negligible MC non-closure.

- Dependence on the choice of the MC model: EPOS LHC [43] is used to generate a different multiplicity response matrix. This response matrix is used to unfold

the N_T and p_T spectra. The ratio between the final unfolded distributions using PYTHIA8 Monash and EPOS LHC was quantified and added to the total systematic uncertainty. In the interval $0 < N_T < 18$, the relative systematic uncertainty is below 2%, increasing to about 4% at $N_T \approx 18$. Due to statistical limitations on the response matrix, a constant 4% relative systematic uncertainty for $N_T \geq 18$ was assigned.

- Track selection: this uncertainty is quantified by changing the track selection criteria with respect to the nominal one. In particular, the minimum number of crossed rows in the TPC is set to 60 and 100 (the nominal is 70). The track fit quality in the ITS and TPC quantified by the $\chi^2_{\mathrm{ITS}}/N_{\mathrm{hits}}$ and the $\chi^2_{\mathrm{TPC}}/N_{\mathrm{clusters}}$ must not exceed 25 and 49 (the nominal is 36), and 3 and 5 (the nominal is 4), respectively. The maximum distance of closest approach to the vertex along the beam axis (DCA_z) is set to 1 and $5\,\mathrm{cm}$ (the nominal is $2\,\mathrm{cm}$). Furthermore, the parameters of the geometrical length cut to select the leading particle are also varied. For a particular parameter variation, the maximum difference between the results obtained with the tighter and looser selections with respect to the nominal value is quantified. The total systematic uncertainty from track variations is given as the sum in quadrature of the different parameter variations. The relative systematic uncertainty is on average 1% in the interval $0 < N_T < 18$ and increases for higher N_T values. For $N_T \geq 18$, the statistical fluctuations become significant. Therefore, a constant 2% relative systematic uncertainty was assigned.

R_T-independent systematic uncertainties. The R_T-independent systematic uncertainties are divided into two categories. The first category includes the uncertainties common to the different analyses, such as those due to the track quality criteria and the p_T-dependent ITS–TPC matching efficiency. The ITS–TPC matching efficiency is derived from matching ITS pure tracks with the corresponding ITS+TPC tracks (in the same phase-space region) and by comparing the matching efficiency in data and Monte Carlo simulations. The second category groups the analysis specific uncertainties. It includes the uncertainties on the secondary particle contamination correction estimation, the signal extraction technique and the TPC–TOF matching efficiency.

As described in section 2.3, the secondary particle contamination correction is based on multi-template fits to the DCA_{xy} distributions in transverse momentum intervals. The estimation of the systematic uncertainty follows the procedure described in [28]. Namely, the fitting range is changed from the nominal values of $\pm 3\,\mathrm{cm}$ to $\pm 1.5\,\mathrm{cm}$.

To estimate possible systematic effects attributed to the signal extraction technique in the TPC analysis, a similar procedure to the one described in [28] was applied. The signal extraction technique changed from fitting n_σ distributions to bin counting in the range of $\pm 3\sigma$. The systematic uncertainty on the particle fractions is given as the difference between the nominal particle fractions and the ones obtained from bin counting.

As described in section 2.2, the measurement of the particle fractions in the TOF analysis is based on fits to β distributions in momentum intervals. Hence, the systematic uncertainty is mainly driven by the uncertainty in the parameterisation of the μ, σ, and ξ curves for π, K, and p. The relative difference between the fitted curves and the actual measured μ, σ, and ξ values was computed to evaluate the effect of the parameterisations.

Thus, the systematic uncertainty in the extraction of the particle fractions is obtained by refitting the β distributions while randomly varying the constrained parameters μ, σ, and ξ within the uncertainty of the parameterisations assuming a Gaussian variation centred at the nominal value. The refitting was performed 1000 times, and the systematic uncertainty on the particle fractions as a function of the transverse momentum is given as the standard deviation of the associated distributions. This approach is motivated by work developed in [28, 33, 35].

The measurement of the systematic uncertainty on the extraction of the particle fractions in the rTPC analysis follows the method from [28, 33, 35]. In this analysis, the primary source of systematic uncertainty comes from the imprecise description of the detector response, namely the Bethe-Bloch and resolution parameterisations. To estimate the systematic effect, the relative difference between the parameterisations and the actual $\langle \mathrm{d}E/\mathrm{d}x \rangle$ and $\sigma_{\mathrm{d}E/\mathrm{d}x}$ values are measured. The particle fractions are measured following a fitting procedure where the constrained parameters, $\langle \mathrm{d}E/\mathrm{d}x \rangle$ and $\sigma_{\mathrm{d}E/\mathrm{d}x}$, are allowed to vary randomly within the uncertainty of the parameterisations. The fitting procedure was repeated 1000 times and the systematic uncertainty in the particle fractions is given as the standard deviation of the associated distributions.

When computing the p_{T}-differential particle ratios, all the systematic uncertainties cancel out in the ratios except those attributed to the signal extraction and feed-down. In the high p_{T} region (rTPC analysis) the procedure described in [33] is used to extract the signal extraction systematic uncertainty on the K/π and p/π ratios directly from fits to the $\mathrm{d}E/\mathrm{d}x$ distributions.

Table 2 lists a summary of the systematic uncertainties at different p_{T} values for the spectra and particle ratios in the transverse region. The table is divided into common and analysis-specific uncertainties. The values in the toward and away regions are the same as those of the transverse region. The only topological-region-dependent uncertainty is the one attributed to the MC non-closure.

4 Results

This section presents the results of the production of π, K, and p as a function of the relative transverse activity classifier, R_{T}. The data are compared with predictions from PYTHIA8 Monash [36], PYTHIA8 with ropes hadronisation model (indicated as PYTHIA8 ropes) [44], HERWIG7 [45, 46], and EPOS LHC [43]. PYTHIA8 with Monash tune is one of the most popular event generators at LHC energies for most observables but lacks the QGP-like effects observed in small collision systems such as strangeness enhancement, while the other three models are known to describe the strangeness enhancement in small collision systems better [8, 44, 47]. Hence, these models allow for testing a broad range of possible dynamic effects. In PYTHIA8 Monash, the soft-inclusive particle production is based on multiple perturbative parton-parton interactions (MPI) [11]. This model also includes a colour reconnection (CR) mechanism [48], allowing each MPI system's partons to be colour connected with a higher-p_{T} MPI system. In particular, PYTHIA8 Monash describes the enhanced p_{T}-differential proton-to-pion ratio at intermediate p_{T} [3] by introducing the

	Uncertainty (%)								
Common source		π			K			p	
p_T (GeV/c)	0.3	2	5	0.3	2	5	0.45	2	5
ITS–TPC matching efficiency	1.4	2.6	2.9	1.4	2.6	2.9	1.4	2.6	2.9
MC non-closure		3.2			3.6			1.5	
MC dependence	1	1.5	1.7	0.9	1.5	1.7	0.9	1.5	2
Track selection		1			1			1	
Analysis-specific		π			K			p	
TPC, p_T (GeV/c)	0.3		0.7	0.3		0.6	0.45		1
PID	0.1		1.8	7.3		5.9	0.1		3.4
Feed-Down	1		0.3	—		—	10		1.1
TOF, p_T (GeV/c)	1		2	1		2	1		2
PID	negl.		1	0.3		3.4	0.2		0.7
Feed-Down	0.3		negl.	—		—	1		0.2
TOF matching efficiency	3		3	6		6	4		4
rTPC, p_T (GeV/c)	3		5	3		5	3		5
PID	0.7		0.6	6.4		2.8	5.8		4.2
Feed-Down	negl.		negl.	—		—	0.2		0.2
Total		π			K			p	
p_T (GeV/c)	0.3	2	5	0.3	2	5	0.45	2	5
Total	3.9	5.5	4.7	8.3	8.3	5.7	10.2	5.3	5.7
Particle ratios					K/π			p/π	
p_T (GeV/c)				0.3	2	5	0.45	2	5
Total				7.4	4.1	3.2	10.1	1.5	4

Table 2. Summary of systematic uncertainties on the π, K, and p p_T spectra. The uncertainties are shown for different representative p_T values. The last two rows show the total systematic uncertainty on the p_T spectra and the p_T-differential particle ratios. These values correspond to the spectra in the transverse region in the $0 \leq R_T < 0.5$ class.

colour reconnection mechanism and does not need to assume the formation of a medium [49]. PYTHIA8 ropes model allows strings to fuse in an environment with a high density of strings and form "colour ropes". Consequently, colour ropes are expected to produce more strange hadrons and baryons, the latter via probabilistic collapses of ropes to string junctions. EPOS LHC is a core-corona model, which assumes the formation of a QGP medium in the high-density core regions in pp collisions. The hadronisation of the corona is based on string fragmentation, while the particles associated with the core are thermally produced (grand-canonical thermal description). In EPOS LHC, particle production in low-multiplicity

$R_{\mathrm{T}} = N_{\mathrm{T}}/\langle N_{\mathrm{T}}\rangle$	N_{T}	Number of events
0–0.5	0–3	2613151
0.5–1.5	4–11	4055410
1.5–2.5	12–18	1302116
2.5–5	19–30	180652
0–5	0–30	8151331

Table 3. Relation between R_{T} intervals and N_{T} classes.

events is mainly dominated by string fragmentation. In contrast, high-multiplicity events are core dominated, and a large production of strange hadrons and baryons is expected. Particle production in the HERWIG7 is based on cluster hadronisation and it has its own colour reconnection mechanism where baryonic clusters are allowed to be produced in a geometric manner. This model also includes a non-perturbative gluon splitting mechanism to create more s$\bar{\mathrm{s}}$ pairs to account for the strangeness enhancement [50].

The p_{T} spectra as a function of R_{T} are normalised to the total number of events in each R_{T} class. The relation between R_{T} intervals and N_{T} classes is given in table 3. The R_{T} distribution is constructed using the unfolded N_{T} distribution for which the $\langle N_{\mathrm{T}}\rangle$ is equal to 7.366 ± 0.002 (stat.). For each R_{T} bin the intervals under the N_{T} column are inclusive meaning that for $0 \leq R_{\mathrm{T}} < 0.5$, N_{T} is equal to 0, 1, 2 or 3.

Figure 3 shows the unfolded N_{T} and R_{T} probability distributions in the transverse region integrated over all the events with the leading particle along with different model predictions. For each model, the $\langle N_{\mathrm{T}}\rangle$ corresponds to the mean value of the corresponding N_{T} spectrum. It is observed that PYTHIA8 Monash and PYTHIA8 ropes give the best qualitative description of the N_{T} distribution, while EPOS LHC (HERWIG7) overestimates (underestimates) the data for $N_{\mathrm{T}} > 10$. However, when R_{T} is computed, all the models underestimate the data for $R_{\mathrm{T}} \gtrsim 2$. This is because the models poorly describe the low-N_{T} region, so they predict larger $\langle N_{\mathrm{T}}\rangle$ values than the measured ones. Finally, the R_{T} probability distribution is compared with the previous ALICE result [14], which used a limited data sample and applied the unfolding at the level of the R_{T} distribution while in the current analysis the R_{T} spectrum is derived from the N_{T} distribution. The new result is in agreement with the previous ALICE measurement within 1.5%.

Figures 4 to 6 show the transverse momentum distributions of π, K, and p as a function of R_{T}. The results in the toward, away, and transverse regions are shown on the left, middle, and right panels, respectively. The lower panels show the ratios between the R_{T}-dependent p_{T} spectra and the R_{T}-integrated p_{T} spectrum. The R_{T}-independent systematic uncertainties cancel out in the ratios. The R_{T}-dependent systematic uncertainties are correlated and cancel out only partly. From the ratios to the R_{T}-integrated spectrum, it is observed that the toward and away regions share a similar feature at low transverse momentum: a depletion of low-p_{T} particles with increasing R_{T}. Furthermore, this effect follows a mass ordering, being larger for heavier particles. This behaviour is reminiscent of radial flow effects, in which the depletion of low-p_{T} particles is compensated by an increasing number of particles at intermediate p_{T}. The particle production in the toward
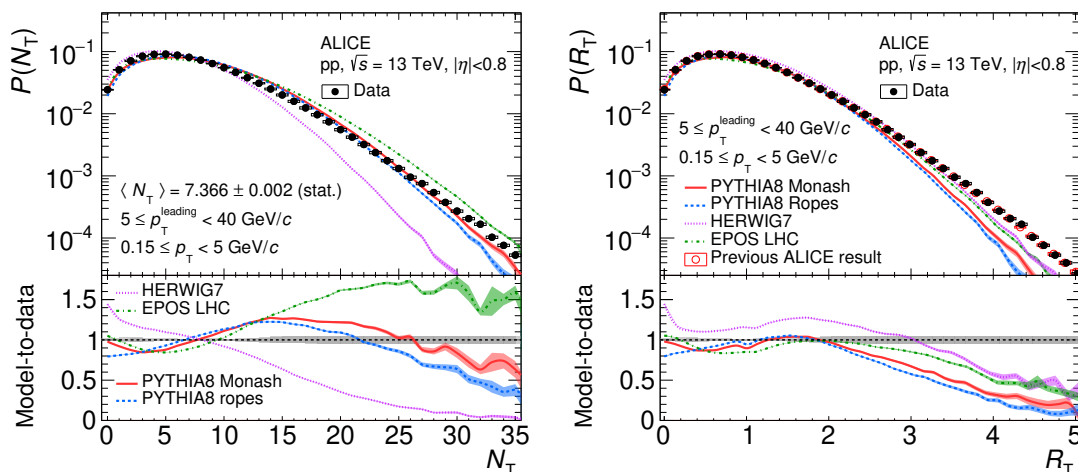
Figure 3. N_T (left) and R_T (right) probability distributions in the transverse region in events with the leading particle. The data are represented with solid black markers and statistical and systematic uncertainties with error bars and boxes, respectively. Model predictions are presented with colour lines and the bands around the model predictions represent only the statistical uncertainty. The bottom panels show the model-to-data ratios. The grey band centred at one in the bottom panel represents the systematic uncertainties of the data.

and away regions is dominated by the leading and away-side jet fragmentation into high-p_T particles. This can be observed in the ratio between the spectra in $0 \leq R_T < 0.5$ and the R_T-integrated ones (bottom panels of figures 4 to 6), which increases with p_T (in the interval $p_T \gtrsim 2\,\mathrm{GeV}/c$), and the effect is more evident for pions. The opposite is observed for the spectral shapes at high R_T; they soften with increasing R_T for $p_T \gtrsim 2\,\mathrm{GeV}/c$. This can be interpreted as a "dilution" of the jet with increasing UE activity. When $R_T \to \infty$ the particle multiplicity from the UE is higher than the particle multiplicity from the jet in the toward region. Thus, average quantities like $\langle p_T \rangle$ of pions and kaons in the toward region decreases at high R_T (see figure 10). The $\langle p_T \rangle$ of protons increases instead with increasing R_T because there other effects like radial flow are more relevant. This can also be seen in the ratios to R_T-integrated spectrum, where they decrease with increasing p_T for events with high UE activity. The spectral shapes of all the species in the transverse region share a common feature: they harden with increasing UE activity. This effect can be attributed to jet hardening with increasing multiplicity.

Figure 7 shows model-to-data ratios for the p_T spectra. The ratios are shown for two types of events: low UE activity ($0 \leq R_T < 0.5$) and high UE activity ($2.5 \leq R_T < 5$). It is observed that the models can describe the pion and kaon spectra for $p_T > 2\,\mathrm{GeV}/c$ in the toward and away regions qualitatively for events with low UE activity. This is expected since for small R_T values, one mainly observes the jet fragmentation products, and the models are tuned to e^+e^- data, which are jet-like. For this same R_T interval, the models predict different yields in the transverse region. However, for $p_T \gtrsim 1\,\mathrm{GeV}/c$ all of the models underestimate the data. Moreover, increasing the UE activity makes the agreement between data and models worse.
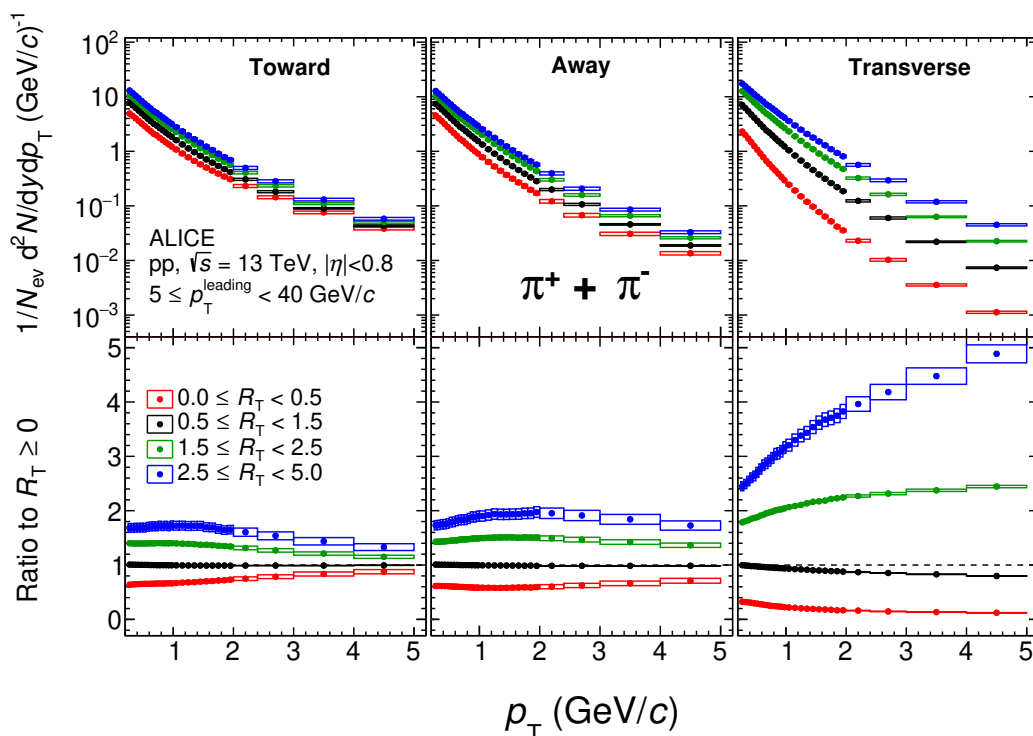
Figure 4. Transverse momentum spectra (top panels) of pions as a function of R_T and ratios to the R_T-integrated spectrum (bottom panels). The toward, away, and transverse regions are shown from left to right. The statistical and systematic uncertainties are represented with bars and boxes, respectively.

Figure 8 shows the p_T-differential kaon-to-pion (K/π) and proton-to-pion (p/π) ratios for the four different R_T intervals in the three topological regions. The R_T-dependent ratios are contrasted with the inclusive ratios in minimum bias collisions at the same centre-of-mass energy [3]. Minimum bias means integrated over R_T and the azimuthal angle, and without the leading particle requirement. The K/π ratios in the toward and away regions show similar features: they increase with increasing UE activity. However, this is true only for $1 \lesssim p_T < 2\,\mathrm{GeV}/c$. Conversely, the K/$\pi$ ratio in the transverse region decreases with increasing R_T. One also observes that the minimum-bias result is very similar to those measured in the transverse region. This suggests that the inclusive K/π ratio is dominated by bulk particle production. The p/π ratio in the toward and away regions measured in the lowest R_T intervals is always below the inclusive one. Similar observations have been made for the $\Lambda/\mathrm{K}^0_\mathrm{S}$ ratio in jets [51]. As the UE increases, the toward and away regions become more UE dominated (jet dilution) and the p/π ratio also increases. However, this is true only for $p_T \gtrsim 1\,\mathrm{GeV}/c$. The growth of the p/$\pi$ ratio might be attributed to a gradual increase of the collective radial flow with R_T. Furthermore, the baryon-to-meson ratio for $p_T > 1\,\mathrm{GeV}/c$ in these two regions tends to increase with increasing R_T and to approach the minimum bias ratio, which is similar to the one measured in the transverse region. The p/π ratio in the transverse region shows a mild dependence on R_T. It is observed that the
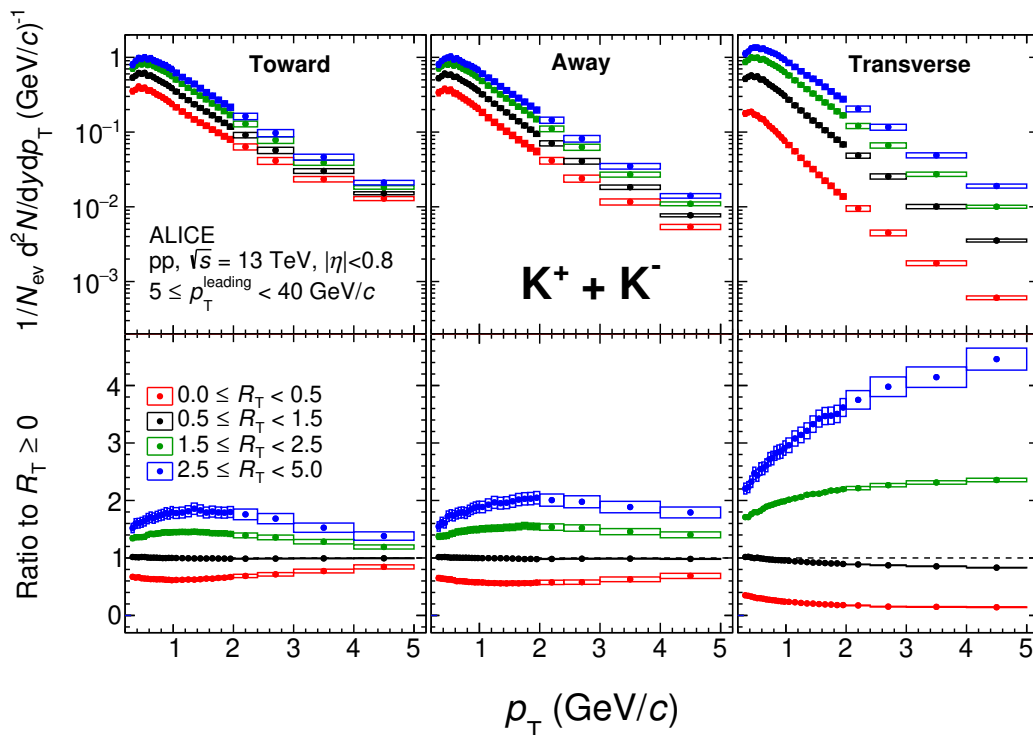
Figure 5. Transverse momentum spectra (top panels) of kaons as a function of R_T and ratios to the R_T-integrated spectrum (bottom panels). The toward, away, and transverse regions are shown from left to right. The statistical and systematic uncertainties are represented with bars and boxes, respectively.

result in the highest UE activity interval is below the one in the lowest UE activity interval for $p_T \lesssim 2\,\mathrm{GeV}/c$, indicating a suppression of low-p_T protons possibly due to collective radial flow. Furthermore, the observed maximum in the highest R_T interval (centred at $p_T \approx 3.5\,\mathrm{GeV}/c$) is shifted to the right with respect to the one of the lowest R_T interval (centred at $p_T \approx 2.5\,\mathrm{GeV}/c$). This might be attributed to the jet hardening effect with increasing multiplicity as discussed in [12].

Figure 9 shows the p_T-differential K/π and p/π ratios along with model predictions in two R_T intervals: $0 \le R_T < 0.5$ (low-UE activity) and $2.5 < R_T < 5$ (high-UE activity). The K/π and p/π ratios in the toward and away regions in events at low R_T can be described qualitatively by PYTHIA8 Monash. However, this model predicts almost no evolution with R_T. On the other hand, the PYTHIA8 ropes hadronisation model, which allows for the formation of colour ropes, predicts p/π ratios that evolve with R_T, but overestimates the data, particularly for high-R_T events. EPOS LHC also describes both ratios qualitatively in the limit of low UE activity and predicts an evolution with R_T. It describes the K/π ratio but overestimates the p/π ratio in events with high R_T. This was clear from the p_T-integrated particle ratios: the transition from string fragmentation to statistical hadronisation needs improvement. Finally, HERWIG7 also predicts an evolution with R_T and can describe rather well the K/π ratio, while it misses the p_T trend of the
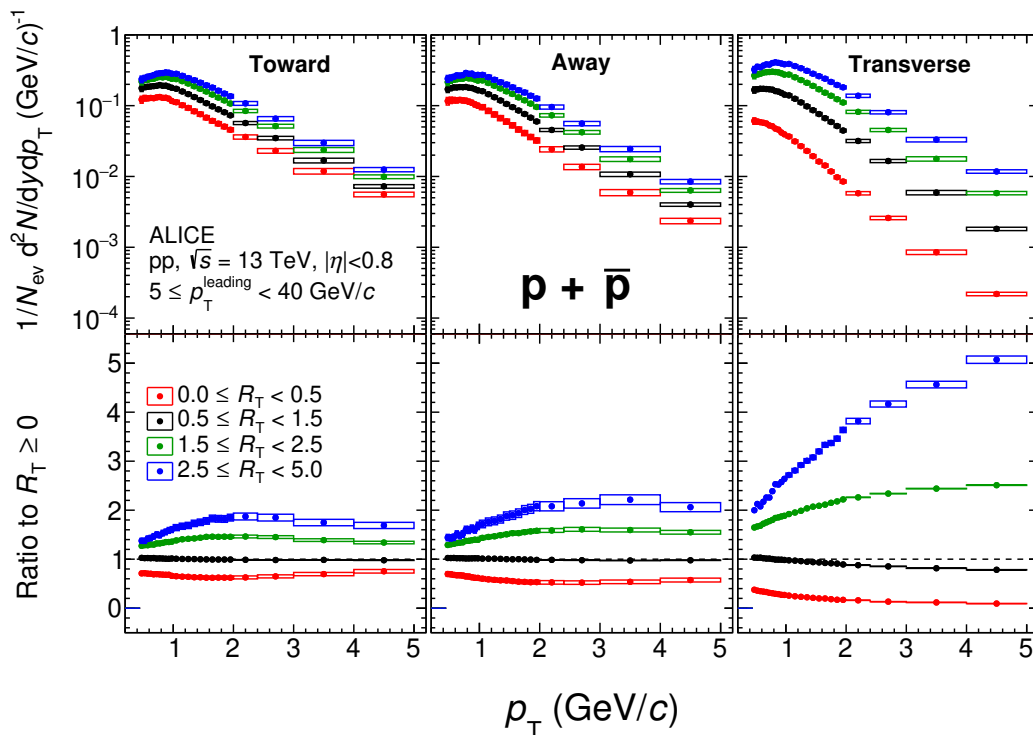
Figure 6. Transverse momentum spectra (top panels) of protons as a function of R_T and ratios to the R_T-integrated spectrum (bottom panels). The toward, away, and transverse regions are shown from left to right. The statistical and systematic uncertainties are represented with bars and boxes, respectively.

p/π ratio. The fact that all models do a better job at describing both ratios at low than at high R_T is expected since they are tuned to e^+e^- data. The model predictions in the away region are similar to those of the toward.

In the transverse region, PYTHIA8 Monash and PYTHIA8 ropes describe the splitting and ordering of the K/π ratio between the two R_T classes qualitatively but underestimate the data. They can also describe the p/π ratio qualitatively. Moreover, those models predict the lower p/π ratio for $p_T \lesssim 2\,\mathrm{GeV}/c$ in events with high R_T compared to the low UE activity ratios. This effect, which can be attributed to the radial flow effects, is likely induced by the CR and ropes in PYTHIA8. EPOS LHC predicts the same K/π ratio for both R_T classes, while the p/π ratio at low R_T agrees with the data. Still, as previously mentioned, the transition from core-corona hadronisation is not well modeled. Finally, HERWIG7 gives a good qualitative description of the evolution of the p/π ratio with R_T in the transverse region.

The p_T-integrated yield (dN/dy) and the average transverse momentum ($\langle p_T \rangle$) of pions, kaons, and protons are extracted from the p_T-differential spectra in the different R_T intervals and topological regions. Since the spectra are measured for $p_T > 0.3\,\mathrm{GeV}/c\ (\pi, \mathrm{K})$ and $p_T > 0.45\ (\mathrm{p})\,\mathrm{GeV}/c$, they are first extrapolated to $p_T = 0$. The extrapolation procedure is carried out by fitting the spectra with Lévy-Tsallis parameterisations [52, 53]. The
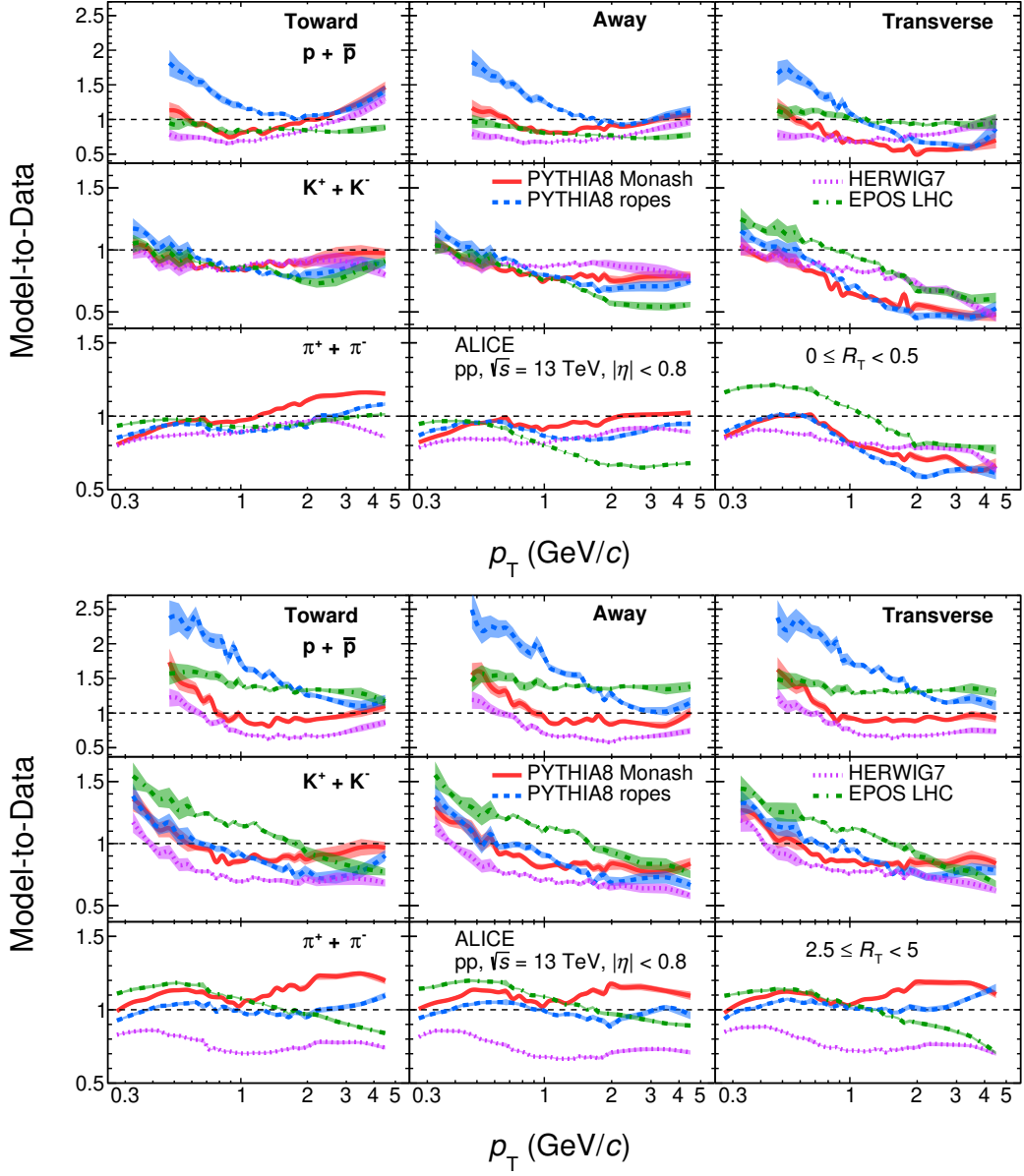
Figure 7. Model-to-data ratios of the transverse momentum spectra. The results are shown for two R_T intervals: $0 \leq R_T < 0.5$ (top figure) and $2.5 \leq R_T < 5$ (bottom figure). The ratios in the toward, away and transverse regions are shown on the left, middle and right column, respectively. The error bands represent the combination of the statistical and systematic uncertainties on the model-to-data ratios.
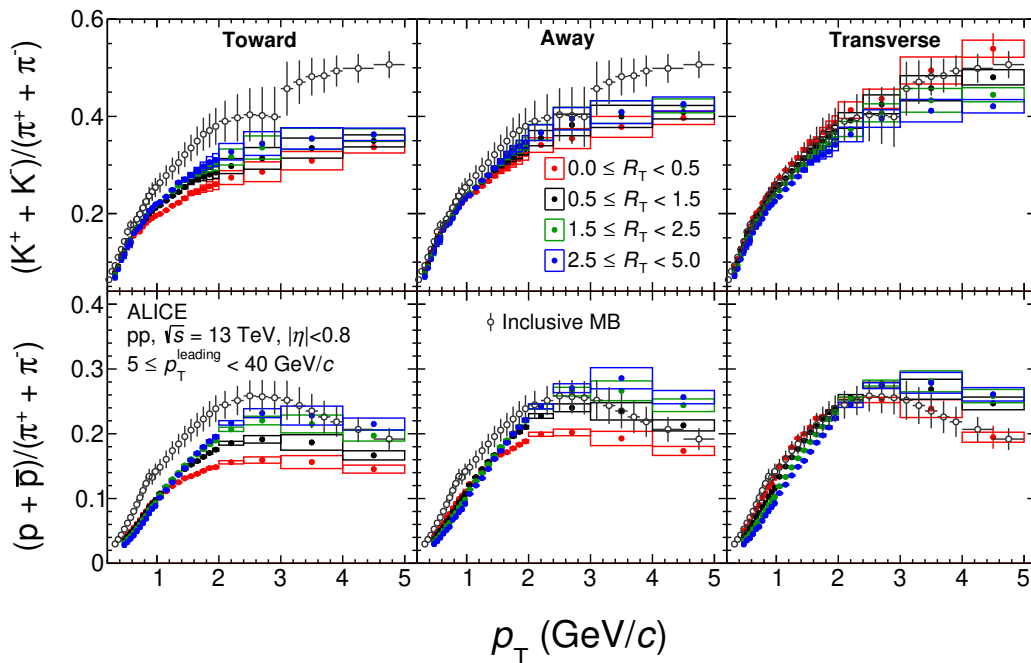
Figure 8. p_T-differential particle ratios as a function of R_T. The top (bottom) row shows the K/π (p/π) ratio. The results in the toward, away, and transverse regions are shown from left to right. Statistical and systematic uncertainties are represented with error bars and boxes, respectively. The inclusive minimum-bias particle ratios in pp collisions at the same centre-of-mass energy [3] are overlaid.

parameterisation is only used in the p_T intervals with no data. For example, for the $0 \leq R_T < 0.5$ interval in the transverse region the fractions of extrapolated yields amount to 38%, 19%, and 22% for π, K, and p, respectively. To estimate the systematic uncertainty associated with the extrapolation procedure, several other parameterisations such as the Fermi-Dirac, Bose-Einstein, Blast-Wave, and m_T-exponential are used to estimate the extrapolated yield. The maximum difference between the nominal and extrapolated yields is associated as the systematic uncertainty of the extrapolation procedure. For example, the systematic uncertainties on the dN/dy ($\langle p_T \rangle$) amount to 2%(1.7%), 2.7%(2.3%), and 2%(1.5%) for π, K, and p, respectively, for the $0 \leq R_T < 0.5$ interval in the transverse region.

Figure 10 shows the average transverse momentum as a function of R_T in the different topological regions. The $\langle p_T \rangle$ of π and K in the toward region is the largest in the $0 \leq R_T < 0.5$ (low UE activity) interval. This feature reflects the presence of the jet fragmenting mainly into low-mass hadrons (π and K) with large transverse momentum. As the UE activity increases, the $\langle p_T \rangle$ of π and K slowly decreases and tends to flatten for $R_T > 1.5$ due to the jet dilution effect: the toward and away regions become dominated by the UE. Conversely, the $\langle p_T \rangle$ of protons increases with R_T, which can be attributed to the additional radial flow effect. Moreover, the $\langle p_T \rangle$ of all the species at high-R_T tend to approach the values measured at high R_T in the transverse region. All models can describe the $\langle p_T \rangle$ qualitatively in the toward region, but EPOS LHC is the only one that predicts an increasing trend of the proton $\langle p_T \rangle$. Particle production in the away region is similar
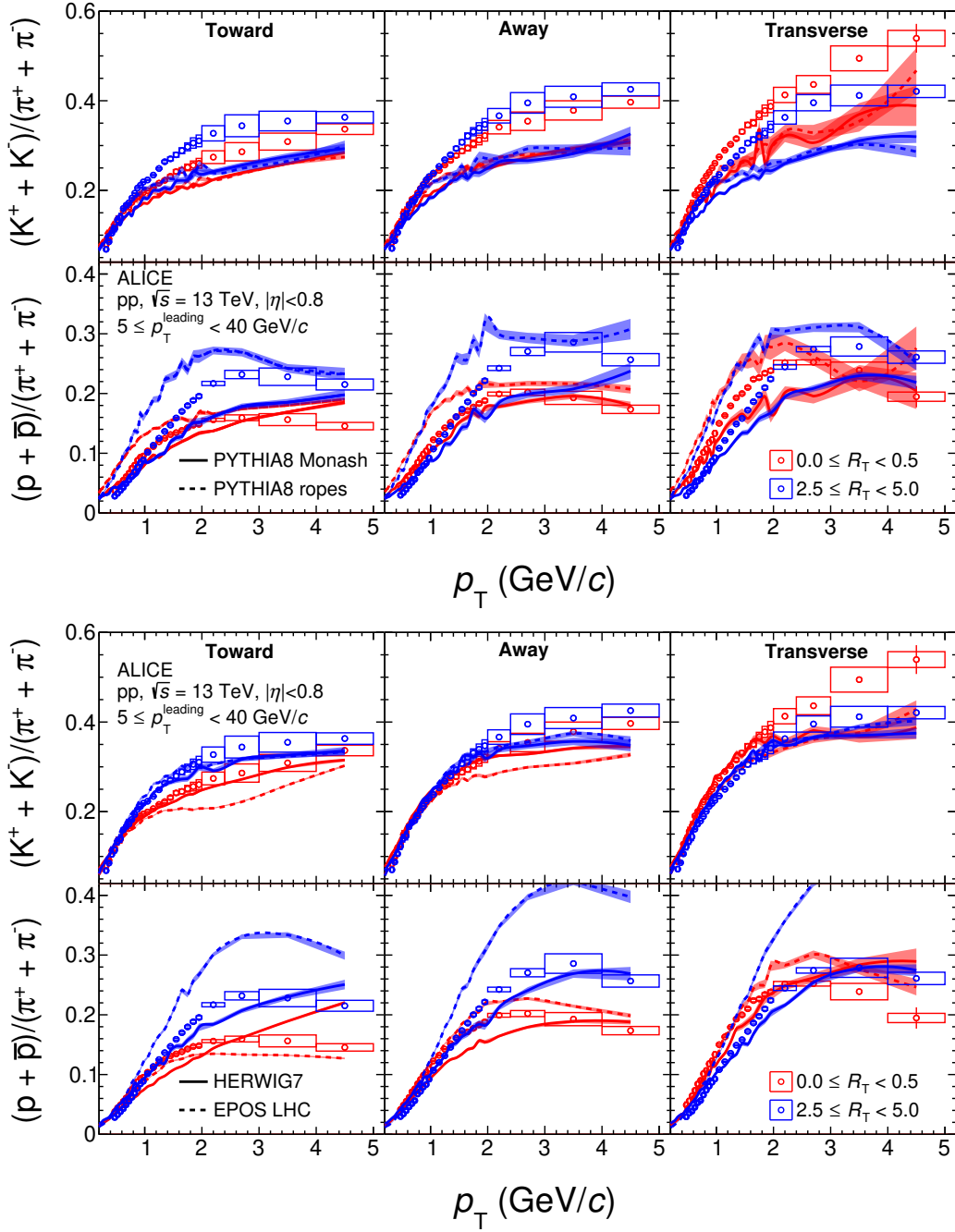
Figure 9. Kaon-to-pion and proton-to-pion ratios as a function of p_T for two R_T intervals: $0 \leq R_T < 0.5$ (red markers) and $2.5 \leq R_T < 5$ (blue markers). The particle ratios in the toward, away and, transverse regions are shown from left to right. The PYTHIA 8 Monash and PYTHIA 8 ropes (EPOS LHC and HERWIG7) predictions are shown in the top (bottom) figure. The shaded regions around the model line represent the statistical uncertainties.
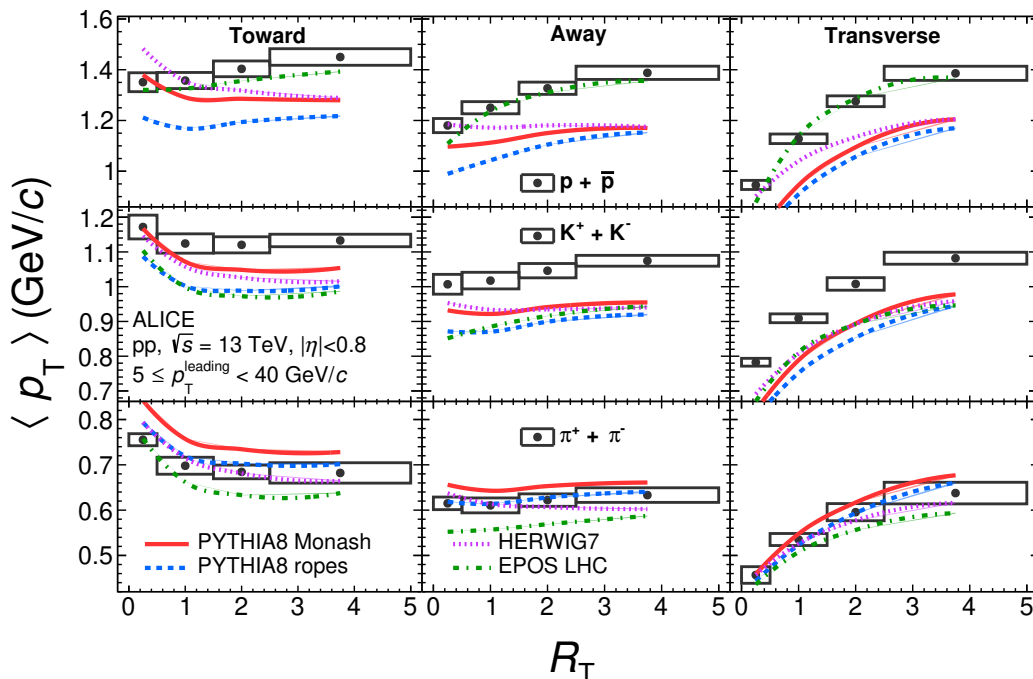
Figure 10. Average transverse momentum as a function of R_T. The $\langle p_T \rangle$ in the toward, away, and transverse regions are shown from left to right. The results for pion, kaon, and protons are shown in the first, second, and third row, respectively. Statistical and systematic uncertainties are represented with error bars and boxes, respectively. The shaded bands around the model lines represent the statistical uncertainties.

to that in the toward. It is primarily dominated by the away-side jet. It is observed that the $\langle p_T \rangle$ of all the species increases with R_T. Furthermore, the $\langle p_T \rangle$ tends to approach the values of the transverse region at large R_T where the UE dominates. PYTHIA8 Monash and ropes give a fair qualitative description of the evolution of $\langle p_T \rangle$ of pions with R_T in the away region while the $\langle p_T \rangle$ of protons in the same region is only described by EPOS LHC.

The $\langle p_T \rangle$ in the transverse region increases with R_T for all the species; however, the rate of increase exhibits a mass ordering, being more significant for heavier particles. Similar observations have been made in multiplicity-dependent studies [2, 3]. The rise of the $\langle p_T \rangle$ with increasing R_T is likely attributed to autocorrelation effects. Since R_T and the p_T spectra are measured in the same $\Delta\varphi$ region, the high multiplicity requirement in the transverse region increases the probability to have a jet in the same region. Finally, it is observed that all the models predict the increase of the $\langle p_T \rangle$ with R_T.

Figure 11 shows the R_T-dependence of the p_T-integrated particle ratios calculated from the extrapolated dN/dy. As the UE activity increases, the yield of kaons and protons relative to that of pions increases in the transverse region and in turn, the particle ratios grow until they saturate at $R_T \approx 1.5$. In contrast, in the toward and away regions the K/π ratio is constant as a function of R_T, while the p/π ratio decreases with increasing UE activity. Furthermore, both ratios in the toward and away regions approach the values of the transverse region at large R_T. All models predict the increasing trend of the particle
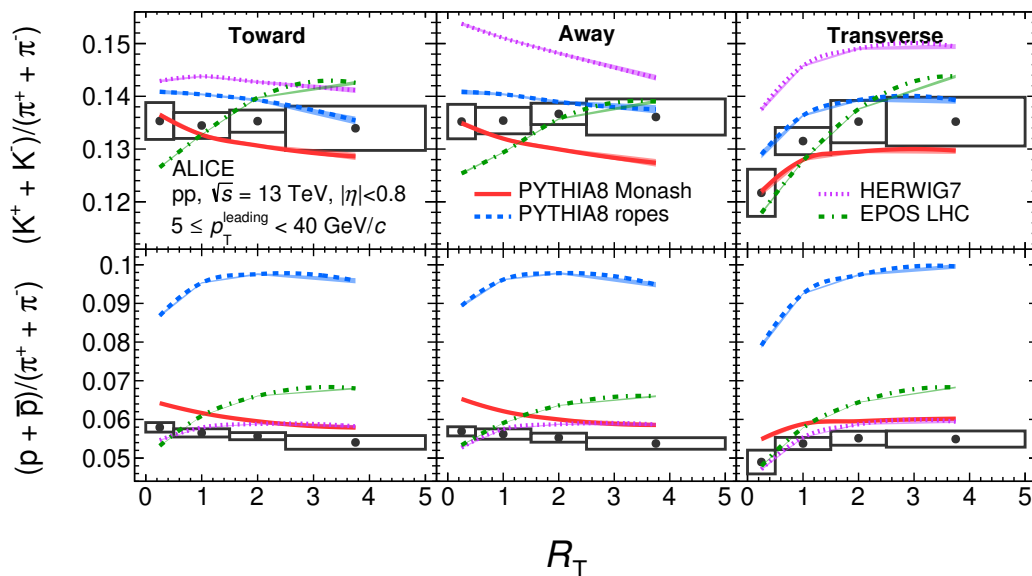
Figure 11. Transverse momentum-integrated particle ratios as a function of R_{T}. The particle ratios in the toward, away, and transverse regions are shown from left to right. The top (bottom) row plots the K/π (p/π). The statistical and systematic uncertainties are represented with error bars and boxes, respectively. The shaded bands around the model lines represent the statistical uncertainties.

ratios with R_{T} in the transverse region. PYTHIA8 Monash and HERWIG7 predict similar p/π ratios to the data. PYTHIA8 ropes overestimates the p/π by a large amount (almost a factor of 2) while EPOS LHC, although overpredicting, is closer to the data. One can notice that while EPOS LHC precisely describes the proton $\langle p_{\mathrm{T}} \rangle$ as a function of R_{T} in all the topological regions, the p/π ratio is only described in the low-UE limit ($0 \leq R_{\mathrm{T}} < 0.5$), where string fragmentation dominates, indicating that the core overestimates the production of protons. PYTHIA8 Monash overpredicts the p/π ratio by about 10 % over the entire R_{T} range and underestimates the K/π ratio. In the toward and away regions none of the models reproduce the trend of both ratios: HERWIG7 and PYTHIA8 Monash predict a strongly decreasing trend for K/π that is not supported by the data. PYTHIA8 ropes and EPOS LHC predict an increasing trend for p/π that is in contradiction with the data. Finally, it is noted that while all the models capture most of the measured trends for $\langle p_{\mathrm{T}} \rangle$ in figure 10, none of the models describes the particle ratio trends of figure 11 for both p/π and K/π.

5 Conclusions

The production of π, K, and p was measured at mid-pseudorapidity in different topological regions as a function of the relative transverse activity classifier, R_{T} in pp collisions at $\sqrt{s} = 13\,\mathrm{TeV}$ containing a high p_{T} ($5 \leq p_{\mathrm{T}}^{\mathrm{leading}} < 40\,\mathrm{GeV}/c$) leading particle. R_{T} has been utilised to investigate differentially in different topological regions where the particle production is expected to be dominantly driven by pQCD-like processes (toward and away

regions and low R_T) and regions where soft non-perturbative QCD processes dominate (transverse region or high R_T). In particular, since conventional UE (Underlying Event) studies average over the event activity, this analysis allows us to get further insight into collective effects and the interplay between hard and soft production in pp collisions. Furthermore, the models can describe the new results in the toward and away regions when the UE is suppressed ($0 \le R_\mathrm{T} < 0.5$), which was expected since they are tuned to reproduce jet-like e^+e^- measurements. However, when the UE increases, all models fail to reproduce the data at both qualitative and quantitative level. This demonstrates that by measuring the production of identified particles as a function of R_T, one can reveal novel features of the UE. The new measurements presented here thus allow for substantial progress on the model side to nail down the properties of the UE.

Acknowledgments

References

[1] CMS collaboration, *Multiplicity and rapidity dependence of strange hadron production in pp, pPb, and PbPb collisions at the LHC*, *Phys. Lett. B* **768** (2017) 103 [arXiv:1605.06699] [INSPIRE].

[2] ALICE collaboration, *Multiplicity dependence of light-flavor hadron production in pp collisions at* $\sqrt{s} = 7$ *TeV*, *Phys. Rev. C* **99** (2019) 024906 [arXiv:1807.11321] [INSPIRE].

[3] ALICE collaboration, *Multiplicity dependence of π, K, and p production in pp collisions at* $\sqrt{s} = 13$ *TeV*, *Eur. Phys. J. C* **80** (2020) 693 [arXiv:2003.02394] [INSPIRE].

[4] ALICE collaboration, *Multiplicity Dependence of Pion, Kaon, Proton and Lambda Production in p-Pb Collisions at* $\sqrt{s_{NN}} = 5.02$ *TeV*, *Phys. Lett. B* **728** (2014) 25 [arXiv:1307.6796] [INSPIRE].

[5] CMS collaboration, *Evidence for collectivity in pp collisions at the LHC*, *Phys. Lett. B* **765** (2017) 193 [arXiv:1606.06198] [INSPIRE].

[6] ALICE collaboration, *Investigations of Anisotropic Flow Using Multiparticle Azimuthal Correlations in pp, p-Pb, Xe-Xe, and Pb-Pb Collisions at the LHC*, *Phys. Rev. Lett.* **123** (2019) 142301 [arXiv:1903.01790] [INSPIRE].

[7] ALICE collaboration, *Multiplicity dependence of (multi-)strange hadron production in proton-proton collisions at* $\sqrt{s} = 13$ *TeV*, *Eur. Phys. J. C* **80** (2020) 167 [arXiv:1908.01861] [INSPIRE].

[8] ALICE collaboration, *Enhanced production of multi-strange hadrons in high-multiplicity proton-proton collisions*, *Nature Phys.* **13** (2017) 535 [arXiv:1606.07424] [INSPIRE].

[9] CMS collaboration, *Measurement of charged pion, kaon, and proton production in proton-proton collisions at* $\sqrt{s} = 13$ *TeV*, *Phys. Rev. D* **96** (2017) 112003 [arXiv:1706.10194] [INSPIRE].

[10] T. Martin, P. Skands and S. Farrington, *Probing Collective Effects in Hadronisation with the Extremes of the Underlying Event*, *Eur. Phys. J. C* **76** (2016) 299 [arXiv:1603.05298] [INSPIRE].

[11] T. Sjöstrand and M. van Zijl, *A Multiple Interaction Model for the Event Structure in Hadron Collisions*, *Phys. Rev. D* **36** (1987) 2019 [INSPIRE].

[12] A. Ortiz, G. Bencedi and H. Bello, *Revealing the source of the radial flow patterns in proton-proton collisions using hard probes*, *J. Phys. G* **44** (2017) 065001 [arXiv:1608.04784] [INSPIRE].

[13] ALICE collaboration, *Mid-rapidity anti-baryon to baryon ratios in pp collisions at* $\sqrt{s} = 0.9$, 2.76 *and* 7 *TeV measured by ALICE*, *Eur. Phys. J. C* **73** (2013) 2496 [arXiv:1305.1562] [INSPIRE].

[14] ALICE collaboration, *Underlying Event properties in pp collisions at* $\sqrt{s} = 13$ *TeV*, *JHEP* **04** (2020) 192 [arXiv:1910.14400] [INSPIRE].

[15] CMS collaboration, *Measurement of the underlying event activity using charged-particle jets in proton-proton collisions at* $\sqrt{s} = 2.76$ *TeV*, *JHEP* **09** (2015) 137 [arXiv:1507.07229] [INSPIRE].

[16] ATLAS collaboration, *Measurement of distributions sensitive to the underlying event in inclusive Z-boson production in pp collisions at* $\sqrt{s} = 7$ *TeV with the ATLAS detector*, *Eur. Phys. J. C* **74** (2014) 3195 [arXiv:1409.3433] [INSPIRE].

[17] CMS collaboration, *Jet and Underlying Event Properties as a Function of Charged-Particle Multiplicity in Proton-Proton Collisions at* $\sqrt{s} = 7$ *TeV*, *Eur. Phys. J. C* **73** (2013) 2674 [arXiv:1310.4554] [INSPIRE].

[18] ATLAS collaboration, *Measurement of the underlying event in jet events from* 7 *TeV proton-proton collisions with the ATLAS detector*, *Eur. Phys. J. C* **74** (2014) 2965 [arXiv:1406.0392] [INSPIRE].

[19] CDF collaboration, *Charged Jet Evolution and the Underlying Event in pp̄ Collisions at 1.8 TeV*, *Phys. Rev. D* **65** (2002) 092002 [INSPIRE].

[20] A. Ortiz, G. Paić and E. Cuautle, *Mid-rapidity charged hadron transverse spherocity in pp collisions simulated with Pythia*, *Nucl. Phys. A* **941** (2015) 78 [arXiv:1503.03129] [INSPIRE].

[21] ALICE collaboration, *Charged-particle production as a function of multiplicity and transverse spherocity in pp collisions at $\sqrt{s} = 5.02$ and 13 TeV*, *Eur. Phys. J. C* **79** (2019) 857 [arXiv:1905.07208] [INSPIRE].

[22] ALICE collaboration, *The ALICE experiment at the CERN LHC*, 2008 *JINST* **3** S08002 [INSPIRE].

[23] ALICE collaboration, *Performance of the ALICE Experiment at the CERN LHC*, *Int. J. Mod. Phys. A* **29** (2014) 1430044 [arXiv:1402.4476] [INSPIRE].

[24] ALICE collaboration, *Performance of the ALICE VZERO system*, 2013 *JINST* **8** P10016 [arXiv:1306.3130] [INSPIRE].

[25] ALICE collaboration, *Alignment of the ALICE Inner Tracking System with cosmic-ray tracks*, 2010 *JINST* **5** P03003 [arXiv:1001.0502] [INSPIRE].

[26] J. Alme et al., *The ALICE TPC, a large 3-dimensional tracking device with fast readout for ultra-high multiplicity events*, *Nucl. Instrum. Meth. A* **622** (2010) 316 [arXiv:1001.1950] [INSPIRE].

[27] A. Akindinov et al., *Performance of the ALICE Time-Of-Flight detector at the LHC*, *Eur. Phys. J. Plus* **128** (2013) 44 [INSPIRE].

[28] ALICE collaboration, *Production of charged pions, kaons and (anti-)protons in Pb-Pb and inelastic pp collisions at $\sqrt{s_{\mathrm{NN}}} = 5.02$ TeV*, *Phys. Rev. C* **101** (2020) 044907 [arXiv:1910.07678] [INSPIRE].

[29] ALICE collaboration, *The ALICE definition of primary particles*, ALICE-PUBLIC-2017-005 (2017).

[30] ALICE collaboration, *Measurement of Event Background Fluctuations for Charged Particle Jet Reconstruction in Pb-Pb collisions at $\sqrt{s_{\mathrm{NN}}} = 2.76$ TeV*, *JHEP* **03** (2012) 053 [arXiv:1201.2423] [INSPIRE].

[31] ALICE collaboration, *Long-range angular correlations on the near and away side in p-Pb collisions at $\sqrt{s_{NN}} = 5.02$ TeV*, *Phys. Lett. B* **719** (2013) 29 [arXiv:1212.2001] [INSPIRE].

[32] ALICE collaboration, *Transverse momentum spectra and nuclear modification factors of charged particles in pp, p-Pb and Pb-Pb collisions at the LHC*, *JHEP* **11** (2018) 013 [arXiv:1802.09145] [INSPIRE].

[33] ALICE collaboration, *Centrality dependence of the nuclear modification factor of charged pions, kaons, and protons in Pb-Pb collisions at $\sqrt{s_{\mathrm{NN}}} = 2.76$ TeV*, *Phys. Rev. C* **93** (2016) 034913 [arXiv:1506.07287] [INSPIRE].

[34] ALICE collaboration, *Production of charged pions, kaons and protons at large transverse momenta in pp and Pb-Pb collisions at $\sqrt{s_{\mathrm{NN}}} = 2.76$ TeV*, *Phys. Lett. B* **736** (2014) 196 [arXiv:1401.1250] [INSPIRE].

[35] ALICE collaboration, *Multiplicity dependence of charged pion, kaon, and (anti)proton production at large transverse momentum in p-Pb collisions at $\sqrt{s_{\mathrm{NN}}} = 5.02$ TeV*, *Phys. Lett. B* **760** (2016) 720 [arXiv:1601.03658] [INSPIRE].

[36] P. Skands, S. Carrazza and J. Rojo, *Tuning PYTHIA 8.1: the Monash 2013 Tune*, *Eur. Phys. J. C* **74** (2014) 3024 [arXiv:1404.5630] [INSPIRE].

[37] R. Brun et al., *GEANT 3: user's guide Geant 3.10, Geant 3.11; rev. version*, CERN-DD-EE-84-01 (1987).

[38] GEANT4 collaboration, *GEANT4 — a simulation toolkit*, *Nucl. Instrum. Meth. A* **506** (2003) 250 [INSPIRE].

[39] A. Ferrari, P.R. Sala, A. Fassò and J. Ranft, *FLUKA: A multi-particle transport code (program version 2005)*, [CERN-2005-010 (2005).

[40] ALICE collaboration, *Centrality dependence of π, K, p production in Pb-Pb collisions at* $\sqrt{s_{NN}} = 2.76$ *TeV*, *Phys. Rev. C* **88** (2013) 044910 [arXiv:1303.0737] [INSPIRE].

[41] G. D'Agostini, *A Multidimensional unfolding method based on Bayes' theorem*, *Nucl. Instrum. Meth. A* **362** (1995) 487 [INSPIRE].

[42] T. Adye, *Unfolding algorithms and tests using RooUnfold*, in the proceedings of the *PHYSTAT 2011*, CERN, Geneva (2011), p. 313–318 [DOI:10.5170/CERN-2011-006.313] [arXiv:1105.1160] [INSPIRE].

[43] T. Pierog et al., *EPOS LHC: Test of collective hadronization with data measured at the CERN Large Hadron Collider*, *Phys. Rev. C* **92** (2015) 034906 [arXiv:1306.0121] [INSPIRE].

[44] C. Bierlich, G. Gustafson, L. Lönnblad and A. Tarasov, *Effects of Overlapping Strings in pp Collisions*, *JHEP* **03** (2015) 148 [arXiv:1412.6259] [INSPIRE].

[45] M. Bahr et al., *Herwig++ Physics and Manual*, *Eur. Phys. J. C* **58** (2008) 639 [arXiv:0803.0883] [INSPIRE].

[46] J. Bellm et al., *Herwig 7.0/Herwig++ 3.0 release note*, *Eur. Phys. J. C* **76** (2016) 196 [arXiv:1512.01178] [INSPIRE].

[47] S. Gieseke, P. Kirchgaeßer and S. Plätzer, *Baryon production from cluster hadronisation*, *Eur. Phys. J. C* **78** (2018) 99 [arXiv:1710.10906] [INSPIRE].

[48] T. Sjöstrand, S. Mrenna and P.Z. Skands, *PYTHIA 6.4 Physics and Manual*, *JHEP* **05** (2006) 026 [hep-ph/0603175] [INSPIRE].

[49] A. Ortiz Velasquez et al., *Color Reconnection and Flowlike Patterns in pp Collisions*, *Phys. Rev. Lett.* **111** (2013) 042001 [arXiv:1303.6326] [INSPIRE].

[50] C.B. Duncan and P. Kirchgaeßer, *Kinematic strangeness production in cluster hadronization*, *Eur. Phys. J. C* **79** (2019) 61 [arXiv:1811.10336] [INSPIRE].

[51] ALICE collaboration, *Production of* Λ *and* K^0_s *in jets in p-Pb collisions at* $\sqrt{s_{NN}} = 5.02$ *TeV and pp collisions at* $\sqrt{s} = 7$ *TeV*, *Phys. Lett. B* **827** (2022) 136984 [arXiv:2105.04890] [INSPIRE].

[52] C. Tsallis, *Possible Generalization of Boltzmann-Gibbs Statistics*, *J. Statist. Phys.* **52** (1988) 479 [INSPIRE].

[53] G. Wilk and Z. Wlodarczyk, *On the interpretation of nonextensive parameter q in Tsallis statistics and Levy distributions*, *Phys. Rev. Lett.* **84** (2000) 2770 [hep-ph/9908459] [INSPIRE].
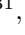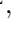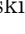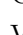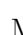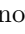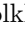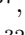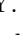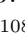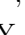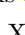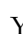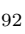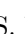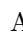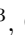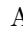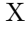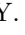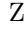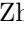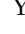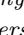
The ALICE collaboration

S. Acharya [125], D. Adamová [86], A. Adler[69], G. Aglieri Rinella [32], M. Agnello [29], N. Agrawal [50], Z. Ahammed [132], S. Ahmad [15], S.U. Ahn [70], I. Ahuja [37], A. Akindinov [140], M. Al-Turany [97], D. Aleksandrov [140], B. Alessandro [55], H.M. Alfanda [6], R. Alfaro Molina [66], B. Ali [15], A. Alici [25], N. Alizadehvandchali [114], A. Alkin [32], J. Alme [20], G. Alocco [51], T. Alt [63], I. Altsybeev [140], M.N. Anaam [6], C. Andrei [45], A. Andronic [135], V. Anguelov [94], F. Antinori [53], P. Antonioli [50], N. Apadula [74], L. Aphecetche [103], H. Appelshäuser [63], C. Arata [73], S. Arcelli [25], M. Aresti [51], R. Arnaldi [55], J.G.M.C.A. Arneiro [110], I.C. Arsene [19], M. Arslandok [137], A. Augustinus [32], R. Averbeck [97], M.D. Azmi [15], A. Badalà [52], J. Bae [104], Y.W. Baek [40], X. Bai [118], R. Bailhache [63], Y. Bailung [47], A. Balbino [29], A. Baldisseri [128], B. Balis [2], D. Banerjee [4], Z. Banoo [91], R. Barbera [26], F. Barile [31], L. Barioglio [95], M. Barlou[78], G.G. Barnaföldi [136], L.S. Barnby [85], V. Barret [125], L. Barreto [110], C. Bartels [117], K. Barth [32], E. Bartsch [63], N. Bastid [125], S. Basu [75], G. Batigne [103], D. Battistini [95], B. Batyunya [141], D. Bauri[46], J.L. Bazo Alba [101], I.G. Bearden [83], C. Beattie [137], P. Becht [97], D. Behera [47], I. Belikov [127], A.D.C. Bell Hechavarria [135], F. Bellini [25], R. Bellwied [114], S. Belokurova [140], V. Belyaev [140], G. Bencedi [136], S. Beole [24], A. Bercuci [45], Y. Berdnikov [140], A. Berdnikova [94], L. Bergmann [94], M.G. Besoiu [62], L. Betev [32], P.P. Bhaduri [132], A. Bhasin [91], M.A. Bhat [4], B. Bhattacharjee [41], L. Bianchi [24], N. Bianchi [48], J. Bielčík [35], J. Bielčíková [86], J. Biernat [107], A.P. Bigot [127], A. Bilandzic [95], G. Biro [136], S. Biswas [4], N. Bize [103], J.T. Blair [108], D. Blau [140], M.B. Blidaru [97], N. Bluhme[38], C. Blume [63], G. Boca [21,54], F. Bock [87], T. Bodova [20], A. Bogdanov[140], S. Boi [22], J. Bok [57], L. Boldizsár [136], A. Bolozdynya [140], M. Bombara [37], P.M. Bond [32], G. Bonomi [131,54], H. Borel [128], A. Borissov [140], A.G. Borquez Carcamo [94], H. Bossi [137], E. Botta [24], Y.E.M. Bouziani [63], L. Bratrud [63], P. Braun-Munzinger [97], M. Bregant [110], M. Broz [35], G.E. Bruno [96,31], M.D. Buckland [23], D. Budnikov [140], H. Buesching [63], S. Bufalino [29], O. Bugnon[103], P. Buhler [102], Z. Buthelezi [67,121], S.A. Bysiak[107], M. Cai [6], H. Caines [137], A. Caliva [97], E. Calvo Villar [101], J.M.M. Camacho [109], P. Camerini [23], F.D.M. Canedo [110], M. Carabas [124], A.A. Carballo [32], F. Carnesecchi [32], R. Caron [126], L.A.D. Carvalho [110], J. Castillo Castellanos [128], F. Catalano [24,29], C. Ceballos Sanchez [141], I. Chakaberia [74], P. Chakraborty [46], S. Chandra [132], S. Chapeland [32], M. Chartier [117], S. Chattopadhyay [132], S. Chattopadhyay [99], T.G. Chavez [44], T. Cheng [97,6], C. Cheshkov [126], B. Cheynis [126], V. Chibante Barroso [32], D.D. Chinellato [111], E.S. Chizzali [II,95], J. Cho [57], S. Cho [57], P. Chochula [32], P. Christakoglou [84], C.H. Christensen [83], P. Christiansen [75], T. Chujo [123], M. Ciacco [29], C. Cicalo [51], F. Cindolo [50], M.R. Ciupek[97], G. Clai [III,50], F. Colamaria [49], J.S. Colburn[100], D. Colella [96,31], M. Colocci [32], M. Concas [IV,55], G. Conesa Balbastre [73], Z. Conesa del Valle [72], G. Contin [23], J.G. Contreras [35], M.L. Coquet [128], T.M. Cormier[I,87], P. Cortese [130,55], M.R. Cosentino [112], F. Costa [32], S. Costanza [21,54], C. Cot [72], J. Crkovská [94], P. Crochet [125], R. Cruz-Torres [74], E. Cuautle[64], P. Cui [6], A. Dainese [53], M.C. Danisch [94], A. Danu [62], P. Das [80], P. Das [4], S. Das [4], A.R. Dash [135], S. Dash [46], A. De Caro [28], G. de Cataldo [49], J. de Cuveland[38], A. De Falco [22], D. De Gruttola [28], N. De

Marco [55], C. De Martin [23], S. De Pasquale [28], S. Deb [47], R.J. Debski [2], K.R. Deja[133], R. Del Grande [95], L. Dello Stritto [28], W. Deng [6], P. Dhankher [18], D. Di Bari [31], A. Di Mauro [32], R.A. Diaz [141,7], T. Dietel [113], Y. Ding [126,6], R. Divià [32], D.U. Dixit [18], Ø. Djuvsland[20], U. Dmitrieva [140], A. Dobrin [62], B. Dönigus [63], J.M. Dubinski[133], A. Dubla [97], S. Dudi [90], P. Dupieux [125], M. Durkac[106], N. Dzalaiova[12], T.M. Eder [135], R.J. Ehlers [87], V.N. Eikeland[20], F. Eisenhut [63], D. Elia [49], B. Erazmus [103], F. Ercolessi [25], F. Erhardt [89], M.R. Ersdal[20], B. Espagnon [72], G. Eulisse [32], D. Evans [100], S. Evdokimov [140], L. Fabbietti [95], M. Faggin [27], J. Faivre [73], F. Fan [6], W. Fan [74], A. Fantoni [48], M. Fasel [87], P. Fecchio[29], A. Feliciello [55], G. Feofilov [140], A. Fernández Téllez [44], L. Ferrandi [110], M.B. Ferrer [32], A. Ferrero [128], C. Ferrero [55], A. Ferretti [24], V.J.G. Feuillard [94], V. Filova[35], D. Finogeev [140], F.M. Fionda [51], F. Flor [114], A.N. Flores [108], S. Foertsch [67], I. Fokin [94], S. Fokin [140], E. Fragiacomo [56], E. Frajna [136], U. Fuchs [32], N. Funicello [28], C. Furget [73], A. Furs [140], T. Fusayasu [98], J.J. Gaardhøje [83], M. Gagliardi [24], A.M. Gago [101], C.D. Galvan [109], D.R. Gangadharan [114], P. Ganoti [78], C. Garabatos [97], J.R.A. Garcia [44], E. Garcia-Solis [9], K. Garg [103], C. Gargiulo [32], K. Garner[135], P. Gasik [97], A. Gautam [116], M.B. Gay Ducati [65], M. Germain [103], C. Ghosh[132], M. Giacalone [50,25], P. Giubellino [97,55], P. Giubilato [27], A.M.C. Glaenzer [128], P. Glässel [94], E. Glimos[120], D.J.Q. Goh[76], V. Gonzalez [134], L.H. González-Trueba [66], M. Gorgon [2], S. Gotovac[33], V. Grabski [66], L.K. Graczykowski [133], E. Grecka [86], A. Grelli [58], C. Grigoras [32], V. Grigoriev [140], S. Grigoryan [141,1], F. Grosa [32], J.F. Grosse-Oetringhaus [32], R. Grosso [97], D. Grund [35], G.G. Guardiano [111], R. Guernane [73], M. Guilbaud [103], K. Gulbrandsen [83], T. Gundem [63], T. Gunji [122], W. Guo [6], A. Gupta [91], R. Gupta [91], S.P. Guzman [44], L. Gyulai [136], M.K. Habib[97], C. Hadjidakis [72], F.U. Haider [91], H. Hamagaki [76], A. Hamdi [74], M. Hamid[6], Y. Han [138], R. Hannigan [108], M.R. Haque [133], J.W. Harris [137], A. Harton [9], H. Hassan [87], D. Hatzifotiadou [50], P. Hauer [42], L.B. Havener [137], S.T. Heckel [95], E. Hellbär [97], H. Helstrup [34], M. Hemmer [63], T. Herman [35], G. Herrera Corral [8], F. Herrmann[135], S. Herrmann [126], K.F. Hetland [34], B. Heybeck [63], H. Hillemanns [32], C. Hills [117], B. Hippolyte [127], F.W. Hoffmann [69], B. Hofman [58], B. Hohlweger [84], G.H. Hong [138], M. Horst [95], A. Horzyk [2], R. Hosokawa[14], Y. Hou [6], P. Hristov [32], C. Hughes[120], P. Huhn[63], L.M. Huhta [115], C.V. Hulse [72], T.J. Humanic [88], A. Hutson [114], D. Hutter [38], J.P. Iddon [117], R. Ilkaev[140], H. Ilyas [13], M. Inaba [123], G.M. Innocenti [32], M. Ippolitov [140], A. Isakov [86], T. Isidori [116], M.S. Islam [99], M. Ivanov[12], M. Ivanov [97], V. Ivanov [140], M. Jablonski [2], B. Jacak [74], N. Jacazio [32], P.M. Jacobs [74], S. Jadlovska[106], J. Jadlovsky[106], S. Jaelani [82], L. Jaffe[38], C. Jahnke[111], M.J. Jakubowska [133], M.A. Janik [133], T. Janson[69], M. Jercic[89], S. Jia [10], A.A.P. Jimenez [64], F. Jonas [87], J.M. Jowett [32,97], J. Jung [63], M. Jung [63], A. Junique [32], A. Jusko [100], M.J. Kabus [32,133], J. Kaewjai[105], P. Kalinak [59], A.S. Kalteyer [97], A. Kalweit [32], V. Kaplin [140], A. Karasu Uysal [71], D. Karatovic [89], O. Karavichev [140], T. Karavicheva [140], P. Karczmarczyk [133], E. Karpechev [140], U. Kebschull [69], R. Keidel [139], D.L.D. Keijdener[58], M. Keil [32], B. Ketzer [42], A.M. Khan [6], S. Khan [15], A. Khanzadeev [140], Y. Kharlov [140], A. Khatun [116,15], A. Khuntia [107], M.B. Kidson[113], B. Kileng [34], B. Kim [16], C. Kim [16], D.J. Kim [115], E.J. Kim [68], J. Kim [138], J.S. Kim [40], J. Kim [68], M. Kim [18,94], S. Kim [17], T. Kim [138], K. Kimura [92], S. Kirsch [63], I. Kisel [38], S. Kiselev [140], A. Kisiel [133], J.P. Kitowski [2], J.L. Klay [5], J. Klein [32], S. Klein [74], C. Klein-Bösing [135],

M. Kleiner [63], T. Klemenz [95], A. Kluge [32], A.G. Knospe [114], C. Kobdaj [105], T. Kollegger [97],
A. Kondratyev [141], N. Kondratyeva [140], E. Kondratyuk [140], J. Konig [63],
S.A. Konigstorfer [95], P.J. Konopka [32], G. Kornakov [133], S.D. Koryciak [2], A. Kotliarov [86],
V. Kovalenko [140], M. Kowalski [107], V. Kozhuharov [36], I. Králik [59], A. Kravčáková [37],
L. Kreis [97], M. Krivda [100,59], F. Krizek [86], K. Krizkova Gajdosova [35], M. Kroesen [94],
M. Krüger [63], D.M. Krupova [35], E. Kryshen [140], V. Kučera [32], C. Kuhn [127],
P.G. Kuijer [84], T. Kumaoka [123], D. Kumar [132], L. Kumar [90], N. Kumar [90], S. Kumar [31],
S. Kundu [32], P. Kurashvili [79], A. Kurepin [140], A.B. Kurepin [140], A. Kuryakin [140],
S. Kushpil [86], J. Kvapil [100], M.J. Kweon [57], J.Y. Kwon [57], Y. Kwon [138], S.L. La Pointe [38],
P. La Rocca [26], Y.S. Lai [74], A. Lakrathok [105], M. Lamanna [32], R. Langoy [119], P. Larionov [32],
E. Laudi [32], L. Lautner [32,95], R. Lavicka [102], T. Lazareva [140], R. Lea [131,54], H. Lee [104],
G. Legras [135], J. Lehrbach [38], R.C. Lemmon [85], I. León Monzón [109], M.M. Lesch [95],
E.D. Lesser [18], M. Lettrich [95], P. Lévai [136], X. Li [10], X.L. Li [6], J. Lien [119], R. Lietava [100],
I. Likmeta [114], B. Lim [24,16], S.H. Lim [16], V. Lindenstruth [38], A. Lindner [45], C. Lippmann [97],
A. Liu [18], D.H. Liu [6], J. Liu [117], I.M. Lofnes [20], C. Loizides [87], S. Lokos [107],
J. Lomker [58], P. Loncar [33], J.A. Lopez [94], X. Lopez [125], E. López Torres [7], P. Lu [97,118],
J.R. Luhder [135], M. Lunardon [27], G. Luparello [56], Y.G. Ma [39], A. Maevskaya [140],
M. Mager [32], T. Mahmoud [42], A. Maire [127], M.V. Makariev [36], M. Malaev [140],
G. Malfattore [25], N.M. Malik [91], Q.W. Malik [19], S.K. Malik [91], L. Malinina [VII,141],
D. Mal'Kevich [140], D. Mallick [80], N. Mallick [47], G. Mandaglio [30,52], V. Manko [140],
F. Manso [125], V. Manzari [49], Y. Mao [6], G.V. Margagliotti [23], A. Margotti [50], A. Marín [97],
C. Markert [108], P. Martinengo [32], J.L. Martinez [114], M.I. Martínez [44], G. Martínez García [103],
S. Masciocchi [97], M. Masera [24], A. Masoni [51], L. Massacrier [72], A. Mastroserio [129,49],
O. Matonoha [75], P.F.T. Matuoka [110], A. Matyja [107], C. Mayer [107], A.L. Mazuecos [32],
F. Mazzaschi [24], M. Mazzilli [32], J.E. Mdhluli [121], A.F. Mechler [63], Y. Melikyan [43,140],
A. Menchaca-Rocha [66], E. Meninno [102,28], A.S. Menon [114], M. Meres [12], S. Mhlanga [113,67],
Y. Miake [123], L. Micheletti [55], L.C. Migliorin [126], D.L. Mihaylov [95], K. Mikhaylov [141,140],
A.N. Mishra [136], D. Miśkowiec [97], A. Modak [4], A.P. Mohanty [58], B. Mohanty [80],
M. Mohisin Khan [V,15], M.A. Molander [43], Z. Moravcova [83], C. Mordasini [95], D.A. Moreira De
Godoy [135], I. Morozov [140], A. Morsch [32], T. Mrnjavac [32], V. Muccifora [48], S. Muhuri [132],
J.D. Mulligan [74], A. Mulliri [22], M.G. Munhoz [110], R.H. Munzer [63], H. Murakami [122],
S. Murray [113], L. Musa [32], J. Musinsky [59], J.W. Myrcha [133], B. Naik [121],
A.I. Nambrath [18], B.K. Nandi [46], R. Nania [50], E. Nappi [49], A.F. Nassirpour [75], A. Nath [94],
C. Nattrass [120], M.N. Naydenov [36], A. Neagu [19], A. Negru [124], L. Nellen [64], S.V. Nesbo [34],
G. Neskovic [38], D. Nesterov [140], B.S. Nielsen [83], E.G. Nielsen [83], S. Nikolaev [140],
S. Nikulin [140], V. Nikulin [140], F. Noferini [50], S. Noh [11], P. Nomokonov [141], J. Norman [117],
N. Novitzky [123], P. Nowakowski [133], A. Nyanin [140], J. Nystrand [20], M. Ogino [76],
A. Ohlson [75], V.A. Okorokov [140], J. Oleniacz [133], A.C. Oliveira Da Silva [120],
M.H. Oliver [137], A. Onnerstad [115], C. Oppedisano [55], A. Ortiz Velasquez [64],
J. Otwinowski [107], M. Oya [92], K. Oyama [76], Y. Pachmayer [94], S. Padhan [46],
D. Pagano [131,54], G. Paić [64], A. Palasciano [49], S. Panebianco [128], H. Park [123], H. Park [104],
J. Park [57], J.E. Parkkila [32], R.N. Patra [91], B. Paul [22], H. Pei [6], T. Peitzmann [58], X. Peng [6],
M. Pennisi [24], L.G. Pereira [65], D. Peresunko [140], G.M. Perez [7], S. Perrin [128], Y. Pestov [140],

V. Petráček [35], V. Petrov [140], M. Petrovici [45], R.P. Pezzi [103,65], S. Piano [56], M. Pikna [12], P. Pillot [103], O. Pinazza [50,32], L. Pinsky [114], C. Pinto [95], S. Pisano [48], M. Płoskoń [74], M. Planinic [89], F. Pliquett [63], M.G. Poghosyan [87], B. Polichtchouk [140], S. Politano [29], N. Poljak [89], A. Pop [45], S. Porteboeuf-Houssais [125], V. Pozdniakov [141], K.K. Pradhan [47], S.K. Prasad [4], S. Prasad [47], R. Preghenella [50], F. Prino [55], C.A. Pruneau [134], I. Pshenichnov [140], M. Puccio [32], S. Pucillo [24], Z. Pugelova [106], S. Qiu [84], L. Quaglia [24], R.E. Quishpe [114], S. Ragoni [14,100], A. Rakotozafindrabe [128], L. Ramello [130,55], F. Rami [127], S.A.R. Ramirez [44], T.A. Rancien [73], M. Rasa [26], S.S. Räsänen [43], R. Rath [50], M.P. Rauch [20], I. Ravasenga [84], K.F. Read [87,120], C. Reckziegel [112], A.R. Redelbach [38], K. Redlich [VI,79], C.A. Reetz [97], A. Rehman [20], F. Reidt [32], H.A. Reme-Ness [34], Z. Rescakova [37], K. Reygers [94], A. Riabov [140], V. Riabov [140], R. Ricci [28], M. Richter [19], A.A. Riedel [95], W. Riegler [32], C. Ristea [62], M. Rodríguez Cahuantzi [44], K. Røed [19], R. Rogalev [140], E. Rogochaya [141], T.S. Rogoschinski [63], D. Rohr [32], D. Röhrich [20], P.F. Rojas [44], S. Rojas Torres [35], P.S. Rokita [133], G. Romanenko [141], F. Ronchetti [48], A. Rosano [30,52], E.D. Rosas [64], K. Roslon [133], A. Rossi [53], A. Roy [47], S. Roy [46], N. Rubini [25], O.V. Rueda [114,75], D. Ruggiano [133], R. Rui [23], B. Rumyantsev [141], P.G. Russek [2], R. Russo [84], A. Rustamov [81], E. Ryabinkin [140], Y. Ryabov [140], A. Rybicki [107], H. Rytkonen [115], W. Rzesa [133], O.A.M. Saarimaki [43], R. Sadek [103], S. Sadhu [31], S. Sadovsky [140], J. Saetre [20], K. Šafařík [35], S.K. Saha [4], S. Saha [80], B. Sahoo [46], R. Sahoo [47], S. Sahoo [60], D. Sahu [47], P.K. Sahu [60], J. Saini [132], K. Sajdakova [37], S. Sakai [123], M.P. Salvan [97], S. Sambyal [91], I. Sanna [32,95], T.B. Saramela [110], D. Sarkar [134], N. Sarkar [132], P. Sarma [41], V. Sarritzu [22], V.M. Sarti [95], M.H.P. Sas [137], J. Schambach [87], H.S. Scheid [63], C. Schiaua [45], R. Schicker [94], A. Schmah [94], C. Schmidt [97], H.R. Schmidt [93], M.O. Schmidt [32], M. Schmidt [93], N.V. Schmidt [87], A.R. Schmier [120], R. Schotter [127], A. Schröter [38], J. Schukraft [32], K. Schwarz [97], K. Schweda [97], G. Scioli [25], E. Scomparin [55], J.E. Seger [14], Y. Sekiguchi [122], D. Sekihata [122], I. Selyuzhenkov [97,140], S. Senyukov [127], J.J. Seo [57], D. Serebryakov [140], L. Šerkšnytė [95], A. Sevcenco [62], T.J. Shaba [67], A. Shabetai [103], R. Shahoyan [32], A. Shangaraev [140], A. Sharma [90], B. Sharma [91], D. Sharma [46], H. Sharma [107], M. Sharma [91], S. Sharma [76], S. Sharma [91], U. Sharma [91], A. Shatat [72], O. Sheibani [114], K. Shigaki [92], M. Shimomura [77], J. Shin [11], S. Shirinkin [140], Q. Shou [39], Y. Sibiriak [140], S. Siddhanta [51], T. Siemiarczuk [79], T.F. Silva [110], D. Silvermyr [75], T. Simantathammakul [105], R. Simeonov [36], B. Singh [91], B. Singh [95], R. Singh [80], R. Singh [91], R. Singh [47], S. Singh [15], V.K. Singh [132], V. Singhal [132], T. Sinha [99], B. Sitar [12], M. Sitta [130,55], T.B. Skaali [19], G. Skorodumovs [94], M. Slupecki [43], N. Smirnov [137], R.J.M. Snellings [58], E.H. Solheim [19], J. Song [114], A. Songmoolnak [105], F. Soramel [27], R. Spijkers [84], I. Sputowska [107], J. Staa [75], J. Stachel [94], I. Stan [62], P.J. Steffanic [120], S.F. Stiefelmaier [94], D. Stocco [103], I. Storehaug [19], P. Stratmann [135], S. Strazzi [25], C.P. Stylianidis [84], A.A.P. Suaide [110], C. Suire [72], M. Sukhanov [140], M. Suljic [32], R. Sultanov [140], V. Sumberia [91], S. Sumowidagdo [82], S. Swain [60], I. Szarka [12], M. Szymkowski [133], S.F. Taghavi [95], G. Taillepied [97], J. Takahashi [111], G.J. Tambave [20], S. Tang [125,6], Z. Tang [118], J.D. Tapia Takaki [116], N. Tapus [124], L.A. Tarasovicova [135], M.G. Tarzila [45], G.F. Tassielli [31], A. Tauro [32], G. Tejeda Muñoz [44], A. Telesca [32], L. Terlizzi [24], C. Terrevoli [114], G. Tersimonov [3], S. Thakur [4], D. Thomas [108], A. Tikhonov [140], A.R. Timmins [114], M. Tkacik [106], T. Tkacik [106],

A. Toia [63], R. Tokumoto[92], N. Topilskaya [140], M. Toppi [48], F. Torales-Acosta[18], T. Tork [72],
A.G. Torres Ramos [31], A. Trifiró [30,52], A.S. Triolo [30,52], S. Tripathy [50], T. Tripathy [46],
S. Trogolo [32], V. Trubnikov [3], W.H. Trzaska [115], T.P. Trzcinski [133], A. Tumkin [140],
R. Turrisi [53], T.S. Tveter [19], K. Ullaland [20], B. Ulukutlu [95], A. Uras [126], M. Urioni [54,131],
G.L. Usai [22], M. Vala[37], N. Valle [21], L.V.R. van Doremalen[58], M. van Leeuwen [84], C.A. van
Veen [94], R.J.G. van Weelden [84], P. Vande Vyvre [32], D. Varga [136], Z. Varga [136],
M. Vasileiou [78], A. Vasiliev [140], O. Vázquez Doce [48], V. Vechernin [140], E. Vercellin [24],
S. Vergara Limón[44], L. Vermunt [97], R. Vértesi [136], M. Verweij [58], L. Vickovic[33], Z. Vilakazi[121],
O. Villalobos Baillie [100], A. Villani [23], G. Vino [49], A. Vinogradov [140], T. Virgili [28],
V. Vislavicius[75], A. Vodopyanov [141], B. Volkel [32], M.A. Völkl [94], K. Voloshin[140],
S.A. Voloshin [134], G. Volpe [31], B. von Haller [32], I. Vorobyev [95], N. Vozniuk [140],
J. Vrláková [37], C. Wang [39], D. Wang[39], Y. Wang [39], A. Wegrzynek [32], F.T. Weiglhofer[38],
S.C. Wenzel [32], J.P. Wessels [135], S.L. Weyhmiller [137], J. Wiechula [63], J. Wikne [19],
G. Wilk [79], J. Wilkinson [97], G.A. Willems [135], B. Windelband[94], M. Winn [128],
J.R. Wright [108], W. Wu[39], Y. Wu [118], R. Xu [6], A. Yadav [42], A.K. Yadav [132], S. Yalcin [71],
Y. Yamaguchi[92], S. Yang[20], S. Yano [92], Z. Yin [6], I.-K. Yoo [16], J.H. Yoon [57], S. Yuan[20],
A. Yuncu [94], V. Zaccolo [23], C. Zampolli [32], F. Zanone [94], N. Zardoshti [32,100],
A. Zarochentsev [140], P. Závada [61], N. Zaviyalov[140], M. Zhalov [140], B. Zhang [6], L. Zhang [39],
S. Zhang [39], X. Zhang [6], Y. Zhang[118], Z. Zhang [6], M. Zhao [10], V. Zherebchevskii [140],
Y. Zhi[10], D. Zhou [6], Y. Zhou [83], J. Zhu [97,6], Y. Zhu[6], S.C. Zugravel [55], N. Zurlo [131,54]

1 *A.I. Alikhanyan National Science Laboratory (Yerevan Physics Institute) Foundation, Yerevan, Armenia*

2 *AGH University of Science and Technology, Cracow, Poland*

3 *Bogolyubov Institute for Theoretical Physics, National Academy of Sciences of Ukraine, Kiev, Ukraine*

4 *Bose Institute, Department of Physics and Centre for Astroparticle Physics and Space Science (CAPSS), Kolkata, India*

5 *California Polytechnic State University, San Luis Obispo, California, United States*

6 *Central China Normal University, Wuhan, China*

7 *Centro de Aplicaciones Tecnológicas y Desarrollo Nuclear (CEADEN), Havana, Cuba*

8 *Centro de Investigación y de Estudios Avanzados (CINVESTAV), Mexico City and Mérida, Mexico*

9 *Chicago State University, Chicago, Illinois, United States*

10 *China Institute of Atomic Energy, Beijing, China*

11 *Chungbuk National University, Cheongju, Republic of Korea*

12 *Comenius University Bratislava, Faculty of Mathematics, Physics and Informatics, Bratislava, Slovak Republic*

13 *COMSATS University Islamabad, Islamabad, Pakistan*

14 *Creighton University, Omaha, Nebraska, United States*

15 *Department of Physics, Aligarh Muslim University, Aligarh, India*

16 *Department of Physics, Pusan National University, Pusan, Republic of Korea*

17 *Department of Physics, Sejong University, Seoul, Republic of Korea*

18 *Department of Physics, University of California, Berkeley, California, United States*

19 *Department of Physics, University of Oslo, Oslo, Norway*

20 *Department of Physics and Technology, University of Bergen, Bergen, Norway*

21 *Dipartimento di Fisica, Università di Pavia, Pavia, Italy*

22 *Dipartimento di Fisica dell'Università and Sezione INFN, Cagliari, Italy*

23 *Dipartimento di Fisica dell'Università and Sezione INFN, Trieste, Italy*

24 *Dipartimento di Fisica dell'Università and Sezione INFN, Turin, Italy*

25 *Dipartimento di Fisica e Astronomia dell'Università and Sezione INFN, Bologna, Italy*

[26] *Dipartimento di Fisica e Astronomia dell'Università and Sezione INFN, Catania, Italy*

[27] *Dipartimento di Fisica e Astronomia dell'Università and Sezione INFN, Padova, Italy*

[28] *Dipartimento di Fisica 'E.R. Caianiello' dell'Università and Gruppo Collegato INFN, Salerno, Italy*

[29] *Dipartimento DISAT del Politecnico and Sezione INFN, Turin, Italy*

[30] *Dipartimento di Scienze MIFT, Università di Messina, Messina, Italy*

[31] *Dipartimento Interateneo di Fisica 'M. Merlin' and Sezione INFN, Bari, Italy*

[32] *European Organization for Nuclear Research (CERN), Geneva, Switzerland*

[33] *Faculty of Electrical Engineering, Mechanical Engineering and Naval Architecture, University of Split, Split, Croatia*

[34] *Faculty of Engineering and Science, Western Norway University of Applied Sciences, Bergen, Norway*

[35] *Faculty of Nuclear Sciences and Physical Engineering, Czech Technical University in Prague, Prague, Czech Republic*

[36] *Faculty of Physics, Sofia University, Sofia, Bulgaria*

[37] *Faculty of Science, P.J. Šafárik University, Košice, Slovak Republic*

[38] *Frankfurt Institute for Advanced Studies, Johann Wolfgang Goethe-Universität Frankfurt, Frankfurt, Germany*

[39] *Fudan University, Shanghai, China*

[40] *Gangneung-Wonju National University, Gangneung, Republic of Korea*

[41] *Gauhati University, Department of Physics, Guwahati, India*

[42] *Helmholtz-Institut für Strahlen- und Kernphysik, Rheinische Friedrich-Wilhelms-Universität Bonn, Bonn, Germany*

[43] *Helsinki Institute of Physics (HIP), Helsinki, Finland*

[44] *High Energy Physics Group, Universidad Autónoma de Puebla, Puebla, Mexico*

[45] *Horia Hulubei National Institute of Physics and Nuclear Engineering, Bucharest, Romania*

[46] *Indian Institute of Technology Bombay (IIT), Mumbai, India*

[47] *Indian Institute of Technology Indore, Indore, India*

[48] *INFN, Laboratori Nazionali di Frascati, Frascati, Italy*

[49] *INFN, Sezione di Bari, Bari, Italy*

[50] *INFN, Sezione di Bologna, Bologna, Italy*

[51] *INFN, Sezione di Cagliari, Cagliari, Italy*

[52] *INFN, Sezione di Catania, Catania, Italy*

[53] *INFN, Sezione di Padova, Padova, Italy*

[54] *INFN, Sezione di Pavia, Pavia, Italy*

[55] *INFN, Sezione di Torino, Turin, Italy*

[56] *INFN, Sezione di Trieste, Trieste, Italy*

[57] *Inha University, Incheon, Republic of Korea*

[58] *Institute for Gravitational and Subatomic Physics (GRASP), Utrecht University/Nikhef, Utrecht, Netherlands*

[59] *Institute of Experimental Physics, Slovak Academy of Sciences, Košice, Slovak Republic*

[60] *Institute of Physics, Homi Bhabha National Institute, Bhubaneswar, India*

[61] *Institute of Physics of the Czech Academy of Sciences, Prague, Czech Republic*

[62] *Institute of Space Science (ISS), Bucharest, Romania*

[63] *Institut für Kernphysik, Johann Wolfgang Goethe-Universität Frankfurt, Frankfurt, Germany*

[64] *Instituto de Ciencias Nucleares, Universidad Nacional Autónoma de México, Mexico City, Mexico*

[65] *Instituto de Física, Universidade Federal do Rio Grande do Sul (UFRGS), Porto Alegre, Brazil*

[66] *Instituto de Física, Universidad Nacional Autónoma de México, Mexico City, Mexico*

[67] *iThemba LABS, National Research Foundation, Somerset West, South Africa*

[68] *Jeonbuk National University, Jeonju, Republic of Korea*

[69] *Johann-Wolfgang-Goethe Universität Frankfurt Institut für Informatik, Fachbereich Informatik und Mathematik, Frankfurt, Germany*

[70] *Korea Institute of Science and Technology Information, Daejeon, Republic of Korea*

[71] *KTO Karatay University, Konya, Turkey*

[72] *Laboratoire de Physique des 2 Infinis, Irène Joliot-Curie, Orsay, France*

[73] *Laboratoire de Physique Subatomique et de Cosmologie, Université Grenoble-Alpes, CNRS-IN2P3, Grenoble, France*

[74] *Lawrence Berkeley National Laboratory, Berkeley, California, United States*

[75] *Lund University Department of Physics, Division of Particle Physics, Lund, Sweden*

[76] *Nagasaki Institute of Applied Science, Nagasaki, Japan*

[77] *Nara Women's University (NWU), Nara, Japan*

[78] *National and Kapodistrian University of Athens, School of Science, Department of Physics, Athens, Greece*

[79] *National Centre for Nuclear Research, Warsaw, Poland*

[80] *National Institute of Science Education and Research, Homi Bhabha National Institute, Jatni, India*

[81] *National Nuclear Research Center, Baku, Azerbaijan*

[82] *National Research and Innovation Agency — BRIN, Jakarta, Indonesia*

[83] *Niels Bohr Institute, University of Copenhagen, Copenhagen, Denmark*

[84] *Nikhef, National institute for subatomic physics, Amsterdam, Netherlands*

[85] *Nuclear Physics Group, STFC Daresbury Laboratory, Daresbury, United Kingdom*

[86] *Nuclear Physics Institute of the Czech Academy of Sciences, Husinec-Řež, Czech Republic*

[87] *Oak Ridge National Laboratory, Oak Ridge, Tennessee, United States*

[88] *Ohio State University, Columbus, Ohio, United States*

[89] *Physics department, Faculty of science, University of Zagreb, Zagreb, Croatia*

[90] *Physics Department, Panjab University, Chandigarh, India*

[91] *Physics Department, University of Jammu, Jammu, India*

[92] *Physics Program and International Institute for Sustainability with Knotted Chiral Meta Matter (SKCM2), Hiroshima University, Hiroshima, Japan*

[93] *Physikalisches Institut, Eberhard-Karls-Universität Tübingen, Tübingen, Germany*

[94] *Physikalisches Institut, Ruprecht-Karls-Universität Heidelberg, Heidelberg, Germany*

[95] *Physik Department, Technische Universität München, Munich, Germany*

[96] *Politecnico di Bari and Sezione INFN, Bari, Italy*

[97] *Research Division and ExtreMe Matter Institute EMMI, GSI Helmholtzzentrum für Schwerionenforschung GmbH, Darmstadt, Germany*

[98] *Saga University, Saga, Japan*

[99] *Saha Institute of Nuclear Physics, Homi Bhabha National Institute, Kolkata, India*

[100] *School of Physics and Astronomy, University of Birmingham, Birmingham, United Kingdom*

[101] *Sección Física, Departamento de Ciencias, Pontificia Universidad Católica del Perú, Lima, Peru*

[102] *Stefan Meyer Institut für Subatomare Physik (SMI), Vienna, Austria*

[103] *SUBATECH, IMT Atlantique, Nantes Université, CNRS-IN2P3, Nantes, France*

[104] *Sungkyunkwan University, Suwon City, Republic of Korea*

[105] *Suranaree University of Technology, Nakhon Ratchasima, Thailand*

[106] *Technical University of Košice, Košice, Slovak Republic*

[107] *The Henryk Niewodniczanski Institute of Nuclear Physics, Polish Academy of Sciences, Cracow, Poland*

[108] *The University of Texas at Austin, Austin, Texas, United States*

[109] *Universidad Autónoma de Sinaloa, Culiacán, Mexico*

[110] *Universidade de São Paulo (USP), São Paulo, Brazil*

[111] *Universidade Estadual de Campinas (UNICAMP), Campinas, Brazil*

[112] *Universidade Federal do ABC, Santo Andre, Brazil*

[113] *University of Cape Town, Cape Town, South Africa*

[114] *University of Houston, Houston, Texas, United States*

[115] *University of Jyväskylä, Jyväskylä, Finland*

[116] *University of Kansas, Lawrence, Kansas, United States*

[117] *University of Liverpool, Liverpool, United Kingdom*

[118] *University of Science and Technology of China, Hefei, China*

[119] *University of South-Eastern Norway, Kongsberg, Norway*

120 *University of Tennessee, Knoxville, Tennessee, United States*

121 *University of the Witwatersrand, Johannesburg, South Africa*

122 *University of Tokyo, Tokyo, Japan*

123 *University of Tsukuba, Tsukuba, Japan*

124 *University Politehnica of Bucharest, Bucharest, Romania*

125 *Université Clermont Auvergne, CNRS/IN2P3, LPC, Clermont-Ferrand, France*

126 *Université de Lyon, CNRS/IN2P3, Institut de Physique des 2 Infinis de Lyon, Lyon, France*

127 *Université de Strasbourg, CNRS, IPHC UMR 7178, F-67000 Strasbourg, France, Strasbourg, France*

128 *Université Paris-Saclay Centre d'Etudes de Saclay (CEA), IRFU, Départment de Physique Nucléaire (DPhN), Saclay, France*

129 *Università degli Studi di Foggia, Foggia, Italy*

130 *Università del Piemonte Orientale, Vercelli, Italy*

131 *Università di Brescia, Brescia, Italy*

132 *Variable Energy Cyclotron Centre, Homi Bhabha National Institute, Kolkata, India*

133 *Warsaw University of Technology, Warsaw, Poland*

134 *Wayne State University, Detroit, Michigan, United States*

135 *Westfälische Wilhelms-Universität Münster, Institut für Kernphysik, Münster, Germany*

136 *Wigner Research Centre for Physics, Budapest, Hungary*

137 *Yale University, New Haven, Connecticut, United States*

138 *Yonsei University, Seoul, Republic of Korea*

139 *Zentrum für Technologie und Transfer (ZTT), Worms, Germany*

140 *Affiliated with an institute covered by a cooperation agreement with CERN*

141 *Affiliated with an international laboratory covered by a cooperation agreement with CERN*

I *Deceased*

II *Also at: Max-Planck-Institut für Physik, Munich, Germany*

III *Also at: Italian National Agency for New Technologies, Energy and Sustainable Economic Development (ENEA), Bologna, Italy*

IV *Also at: Dipartimento DET del Politecnico di Torino, Turin, Italy*

V *Also at: Department of Applied Physics, Aligarh Muslim University, Aligarh, India*

VI *Also at: Institute of Theoretical Physics, University of Wroclaw, Poland*

VII *Also at: An institution covered by a cooperation agreement with CERN*